Cell

CD1 lipidomes reveal lipid-binding motifs and size-based antigen-display mechanisms

Graphical abstract

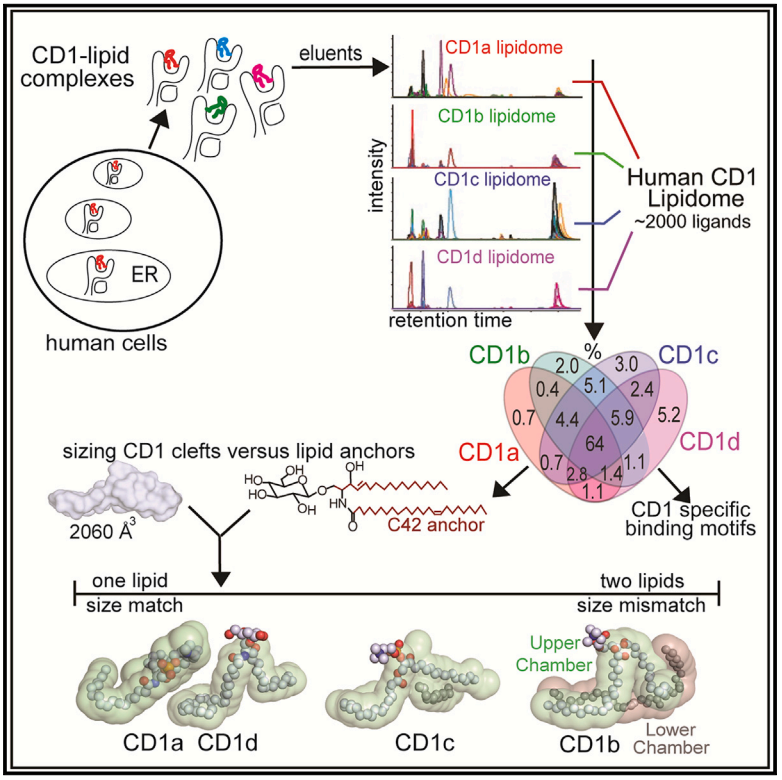

Highlights

- Human CD1 antigen-presenting molecules display >2,000 cellular self-lipids to T cells
- Cellular CD1 proteins edit the self-lipidome by selectively capturing certain lipids
- Unlike MHC-peptide complexes, CD1 often presents lipids in an unprocessed form
- Antigenic capture patterns of each CD1 protein type differ in lipid size, stoichiometry, and chemical structure

Authors

Shouxiong Huang, Adam Shahine, Tan-Yun Cheng, ..., Jacob A. Mayfield, Jamie Rossjohn, D. Branch Moody

Correspondence

shouxiong.huang@uc.edu (S.H.), jamie.rossjohn@monash.edu (J.R.), bmoody@bwh.harvard.edu (D.B.M.)

In brief

Antigen presentation to T cells is often studied in the context of proteins. Analyses of nearly 2,000 distinct human CD1 antigen complexes demonstrate broad sampling of self-cellular lipids for display to T cells, where each CD1 protein captures lipid ligands that differ in size, stoichiometry, and chemical structure.these general lipid motifs can be compared to lipids that contribute to disease, providing new biomedical insights.

Huang et al., 2023, Cell *186*, 1–14
October 12, 2023
https://doi.org/10.1016/j.cell.2023.08.022

CellPress

Cell

CellPress
OPEN ACCESS

Article

CD1 lipidomes reveal lipid-binding motifs and size-based antigen-display mechanisms

Shouxiong Huang,[1,9,*] Adam Shahine,[2,3,9] Tan-Yun Cheng,[1] Yi-Ling Chen,[4,7] Soo Weei Ng,[4] Gautham R. Balaji,[2] Rachel Farquhar,[2,3] Stephanie Gras,[2,3] Clare S. Hardman,[4] John D. Altman,[5] Nabil Tahiri,[6] Adriaan J. Minnaard,[6] Graham S. Ogg,[4,7] Jacob A. Mayfield,[1] Jamie Rossjohn,[2,3,8,9,*] and D. Branch Moody[1,9,10,*]

[1]Division of Rheumatology, Immunity and Inflammation, Brigham and Women's Hospital, Harvard Medical School, Boston, MA 02115, USA
[2]Infection and Immunity Program and Department of Biochemistry and Molecular Biology, Biomedicine Discovery Institute, Monash University, Clayton, VIC 3800, Australia
[3]Australian Research Council Centre of Excellence for Advanced Molecular Imaging, Monash University, Clayton, VIC 3800, Australia
[4]MRC Human Immunology Unit, Weatherall Institute for Molecular Medicine, University of Oxford, Headington, Oxford OX3 9DS, UK
[5]Emory Vaccine Center, Emory School of Medicine, Atlanta, GA 30322, USA
[6]Department of Chemical Biology, Stratingh Institute for Chemistry, Groningen, the Netherlands
[7]Chinese Academy of Medical Sciences Oxford Institute, University of Oxford, Oxford, UK
[8]Institute of Infection and Immunity, Cardiff University, School of Medicine, Heath Park, Cardiff CF14 4XN, UK
[9]These authors contributed equally
[10]Lead contact
*Correspondence: shouxiong.huang@uc.edu (S.H.), jamie.rossjohn@monash.edu (J.R.), bmoody@bwh.harvard.edu (D.B.M.)
https://doi.org/10.1016/j.cell.2023.08.022

SUMMARY

The CD1 system binds lipid antigens for display to T cells. Here, we solved lipidomes for the four human CD1 antigen-presenting molecules, providing a map of self-lipid display. Answering a basic question, the detection of >2,000 CD1-lipid complexes demonstrates broad presentation of self-sphingolipids and phospholipids. Whereas peptide antigens are chemically processed, many lipids are presented in an unaltered form. However, each type of CD1 protein differentially edits the self-lipidome to show distinct capture motifs based on lipid length and chemical composition, suggesting general antigen display mechanisms. For CD1a and CD1d, lipid size matches the CD1 cleft volume. CD1c cleft size is more variable, and CD1b is the outlier, where ligands and clefts show an extreme size mismatch that is explained by uniformly seating two small lipids in one cleft. Furthermore, the list of compounds that comprise the integrated CD1 lipidome supports the ongoing discovery of lipid blockers and antigens for T cells.

INTRODUCTION

Biologists' understanding of T cell responses is centrally informed by T cell receptor (TCR) interactions with peptide antigens bound to major histocompatibility complex (MHC)-encoded proteins.[1,2] A parallel cellular system for antigen display to T cells involves the capture of lipids[3] by mammalian antigen-presenting molecules known as CD1.[4] Although much CD1 research focuses on invariant natural killer T (NKT) cells[5] that recognize α-galactosyl ceramide[6] and CD1d,[7] other CD1-reactive T cells express diverse TCRs that recognize small molecules, sphingolipids, phospholipids, glycolipids, lipopeptides, and phosphoglycolipids.[8] Human cells express CD1e,[9] a soluble lipid transfer protein, and four transmembrane antigen-presenting molecules: CD1a, CD1b, CD1c, and CD1d. These CD1 protein types, known as isoforms, fold to create narrow portals leading to internal hydrophobic clefts that bind the alkyl chains of amphipathic lipids.[10–13] This mode of binding positions the phosphate, carbohydrate, and other hydrophilic head groups on the surface of CD1, where they serve as epitopes for TCR contact.[14]

Human CD1 proteins fold in the endoplasmic reticulum (ER), where all four CD1 isoforms bind β2-microglobulin (β2m)[15] and self-lipids,[16] prior to transiting the secretory pathway to the cell surface.[17] Then, tyrosine-based (YXXZ) cytoplasmic tail motifs divert CD1 proteins through differing endosomal-recycling pathways based on the presence of two (CD1b),[18] one (CD1c, CD1d),[19] or no (CD1a)[20] targeting motifs. For CD1b, lipid length defines two loading mechanisms that occur in different cellular subcompartments. Antigens with short (C32) lipid anchors readily exchange onto CD1b proteins at neutral pH and on the cell surface, but larger (~C80) lipid anchors strictly require low pH and other endosomal factors.[21]

Lipid ligands eluted from individual CD1 isoforms have been detected by mass spectrometry (MS),[22–26] but quantitative methods to enumerate bound lipids or systematically compare ligands across CD1 isoforms were lacking. Detecting natural lipids bound to cellular CD1 proteins in high throughput might

Please cite this article in press as: Huang et al., CD1 lipidomes reveal lipid-binding motifs and size-based antigen-display mechanisms, Cell (2023), https://doi.org/10.1016/j.cell.2023.08.022

answer basic biological questions relating to whether the four CD1 isoforms capture the same or different lipids, or whether CD1 proteins are specific "lipid receptors" that favor binding only certain antigenic structures, like α-hexosylceramides, or instead broadly survey the cellular lipidome. Precedents in the MHC-peptide system suggest that ligand elution provides essential information about the chemical features that render certain molecules capturable and antigenic.[27,28] The microsequencing[29] of MHC bound peptides revealed length- and sequence-based capture motifs,[30] including nonamer peptides matching the length of the MHC class I groove,[31,32] whereas open-ended MHC class II grooves capture longer peptides[28] with ragged ends.[33] These capture motifs later emerged as essential for translational research in autoimmunity, infection, and vaccines because they represent the key tools needed for epitope mapping and otherwise predict which particular molecules will be recognized by T cells.[34] The enclosed nature of CD1 clefts predicts that size motifs for lipid anchors might exist, and if so, the nearly non-polymorphic nature of CD1 proteins means that any solved motifs would apply to all humans.

Building on earlier methods that separate cellular lipids in one chromatographic system,[35] here, we report a sensitive lipidomics platform to broadly detect, enumerate, and chemically define the lipids that form CD1-lipid complexes in cells. We found that the CD1 system provides broad self-lipid sampling rather than the capture of a few chemically dominant ligands. However, elution patterns define capture preferences based on lipid length and other chemical structures that represent motifs for CD1a, CD1b, CD1c, and CD1d proteins. Furthermore, these capture patterns, validated by CD1-lipid crystal structures bound to diverse endogenous lipids, identified three general models of lipid capture by individual CD1 proteins, based on whether lipids are matched in size to the cleft volume. Looking forward, this integrated CD1 lipidomic map can guide the investigation of lipid T cell antigens and cleft blockers in any cellular system or disease.

RESULTS

Cellular expression of human CD1 proteins

Here, we sought to understand self-lipid capture by the four types of human CD1 antigen-presenting molecules, acting on equivalent cellular lipid pools . Detergent extraction of transmembrane proteins displaces lipids from CD1 clefts, a problem that is bypassed by generating soluble proteins with transmembrane domain truncation (Figure S1).[22–25,36,37] Truncation allows protein capture in detergent-free systems and removes YXXZ tail sequences, ensuring that comparative analysis of capture events in the secretory pathway is not confounded by endosomal recycling events that differ by isoform.

We generated two sets of CD1a, CD1b, CD1c, CD1d, and MHC class I control proteins. Five "linked" proteins used a peptide linker for β2m, whereas five "unlinked" proteins contained native or leucine-zippered β2m (Figure S1A). Separate analysis of two protein sets assessed potential confounders related to cell type (K562 versus 293T), protein linker design, and protein capture tags (Figure 1A). Also, the use of K562 and 293T cells leveraged extensive prior validation experiments: K562 cells expressing recombinant CD1a, CD1b, CD1c, and CD1d proteins are equivalent to dendritic cells for lipid display.[38] 293T cells produce CD1 proteins that efficiently bind lipids for presentation to TCRs when affixed to plates or assembled as tetramers.[39–43]

Assembling two human CD1-lipidomes

After cell secretion and affinity purification of CD1-lipid complexes, ligands were eluted with an adapted Folch extraction[44] to generate lipidomes. Complex lipid eluents were separated with normal phase high-performance liquid chromatography with quadrupole time of flight MS (HPLC-QToF-MS).[35,36] The linked and unlinked lipidomes are valid if MS signals derive from self-lipids loaded inside CD1 within cells, rather than eluting from the CD1 surface or exchanging from media. We directly measured lipid exchange from media using exogenous deuterated sphingomyelin (SM) (100 μg/L) and phosphatidylcholine (PC) (2.5 mg/L) at concentrations normally present in serum, which demonstrated trace (CD1c-PC) or no (CD1d-SM) detectable CD1 binding under conditions in which strong endogenous lipid signals were present (Figures 1B, S2A, and S2B).

Unlike direct extraction of cellular lipids,[35] solving CD1-lipidomes required sensitive detection of scant lipids released from cell-derived proteins. Therefore, we updated first-generation, tiered methods to achieve a sensitive, single-step method for the direct analysis of unmanipulated eluents. Normal-phase HPLC-MS with a steep solvent gradient resolved hundreds of ion chromatograms corresponding to hydrophobic lipids, glycolipids, and phospholipids (Figures 1C and 1D). Unlike shotgun methods, chromatography reduces simultaneous ionization to limit cross-suppression and demonstrates the chemical breadth of eluted lipids with more than 1,000 total ion chromatograms per isoform.[45] Endpoints measured are "molecular features," which are ion chromatograms with linked accurate mass, retention time, and intensity values (Figure 1C). Although chemically unnamed, features are reliably tracked based on mass values and represent countable data points that can answer overarching questions. Do CD1 proteins capture few or many distinct lipids? Do the four CD1 protein types capture overlapping or distinct lipid profiles? Answering other questions required chemical naming, so collision-induced dissociation (CID)-MS (Figure S2) identified lipids in the second stage of analysis (Figure 2).

Enumerating cellular ligands of CD1

The four CD1 isoforms might bind a limited spectrum of lipids and fulfill separate roles based on the type of lipid captured, like retinol receptors or fatty acid-binding proteins.[46] At the other extreme, each CD1 isoform might promiscuously bind nearly every cellular lipid so that each protein acts redundantly. Published data highlight the unresolved nature of these questions: an early study detected glycosylphosphatidylinositol as the ligand for CD1d[26] and later MS analyses of CD1a, CD1c, or CD1d detected additional lipids in eluents.[22,23,25] In prior methods, mass spectra showed signal at all *m/z* values, so ligands could not be counted due to threshold-related confounders. By contrast, molecular features are countable because chromatograms must be reproducibly detected in narrow mass and time windows with a defined curve shape (Figure 1C). Alignment of eluents from all CD1 isoforms yielded

Please cite this article in press as: Huang et al., CD1 lipidomes reveal lipid-binding motifs and size-based antigen-display mechanisms, Cell (2023), https://doi.org/10.1016/j.cell.2023.08.022

CellPress
OPEN ACCESS

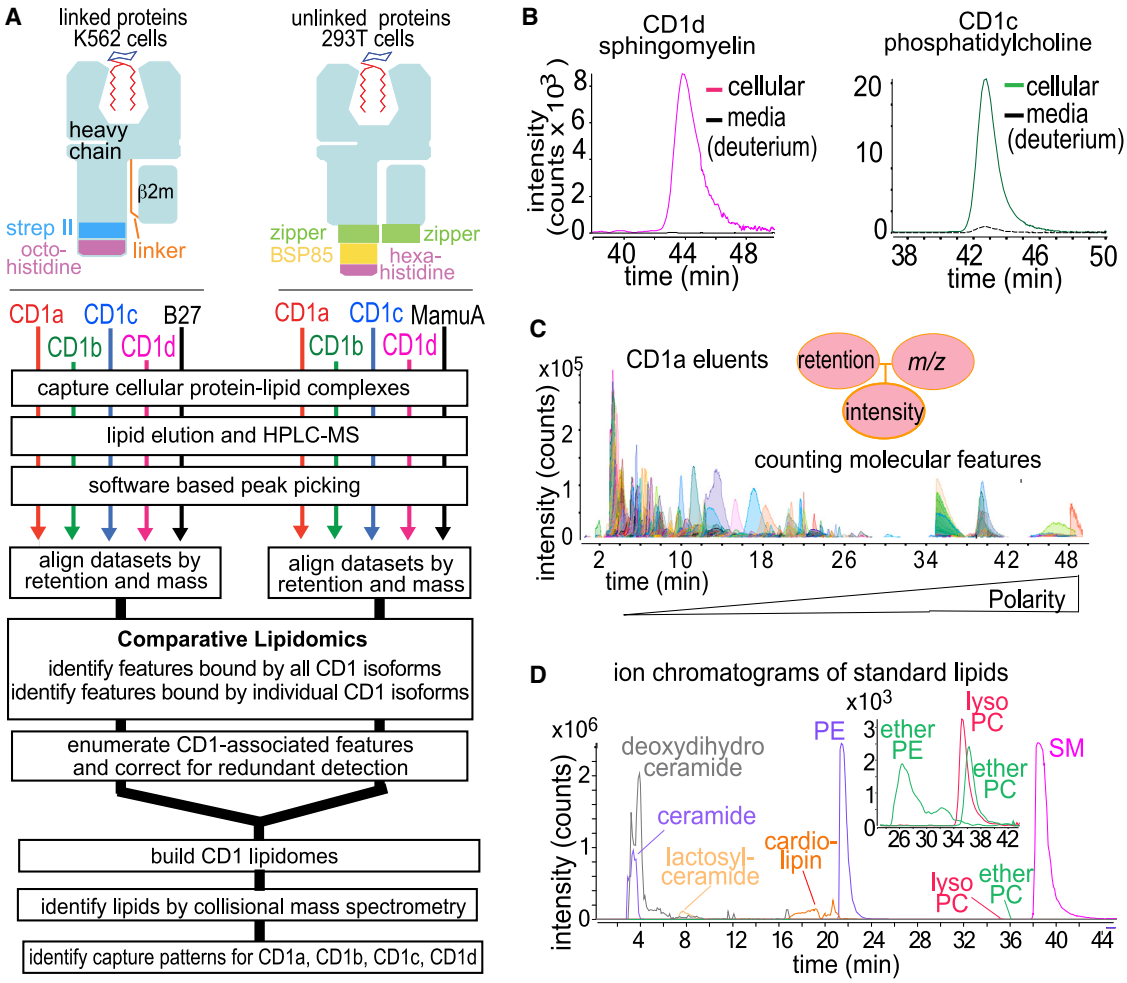

Figure 1. A human CD1-lipidome

(A) Human CD1 and MHC heavy chain genes from human leukocyte antigen B27 (HLA-B27) and *Macaca mulatta* A01 (MamuAwere expressed with strep tag II (strep II), birA substrate peptide 85 (bsp85), polyhistidine tags, zippers, or peptide linkers for β2-microglobulin (β2m).[37] Extracellular secreted complexes were extracted to detect bound lipids via HPLC-QToF-MS-based lipidomics.

(B) To measure media-derived lipids, K562 cells expressing CD1c or CD1d proteins were cultured with deuterated SM (*m/z* 734.767) or PC (*m/z* 791.777), followed by HPLC-MS detection of endogenous SM (*m/z* 703.575) and PC (*m/z* 760.586).

(C) Representative CD1a eluents analyzed in positive mode show discrete, countable ion chromatograms with linked *m/z*, retention time, and intensity values.

(D) Extracted ion chromatograms of standards serve as benchmarks to identify lipids and illustrate the detection of increasingly polar lipid ligands during the run.

See also Figures S1 and S2

1,668 and 1,773 total events in the two datasets (Figure 2B), which is higher than a preliminary estimate.[36]

MHC proteins, HLA-B27 and MamuA, are similar to CD1 in size and structure but lack a hydrophobic cleft.[4,15] With <2% of uncensored events deriving from MHC controls (Figure 2A, red), nearly all events in CD1 eluents likely derive from lipid-binding clefts. To minimize false positive detection, data filters required that events be detected in at least two samples, and that they show >10-fold higher intensity than blanks and generate >2,000 counts. We censored alternative adducts, multimers and isotopes, peak splitting errors, and ions that were not significantly increased in CD1 compared with MHC controls (Figure 2A, gray). The resulting list of "unique features" estimates how many unique CD1 ligands were captured in cells: 404–580 lipids per CD1 isoform (Figure 2B; Tables S1 and S2). The sum of unique CD1-lipid pairs was 1,841 and 2,256 in the two lipidomes, resolving a longstanding question in favor of broad sampling of the cellular lipid pool by the CD1 system.

To estimate isoform overlap, lipidomes were divided into bins based on whether each event was captured by 1, 2, 3, or 4 CD1 isoforms (Figure 2C). We found similar outcomes in linked and unlinked lipidomes: >half of events associated with any isoform bound all 4 isoforms. The breadth and overlapping nature of isoform-specific patterns supported two conclusions: the four CD1 isoforms bind many lipids in ways that could support immunosurveillance, and overlap among the four isoforms shows that they are not like four distinct lipid receptors with non-overlapping ligand profiles.

Please cite this article in press as: Huang et al., CD1 lipidomes reveal lipid-binding motifs and size-based antigen-display mechanisms, Cell (2023), https://doi.org/10.1016/j.cell.2023.08.022

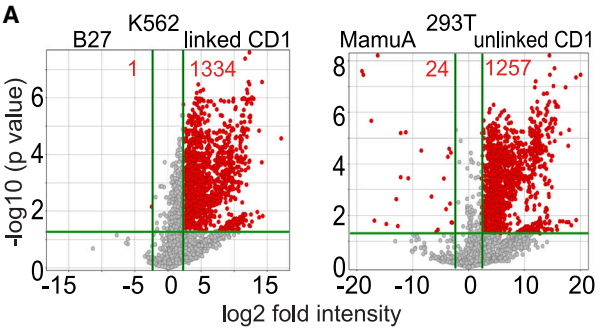

B

	linked CD1 features		unlinked CD1 features	
	total	unique	total	unique
any CD1	1668	542	1773	631
CD1a	1216	460	1336	549
CD1b	1361	494	1490	568
CD1c	1341	483	1561	580
CD1d	1104	404	1486	559
total CD1-lipid pairs		1841		2256

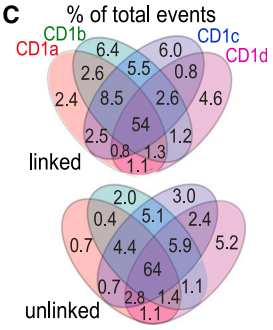

Figure 2. Scope of the human CD1 lipidome and patterns of CD1 isoform specificity

(A) To determine non-specific lipid adherence to proteins, events with equivalent *m/z* and retention time values generate intensity ratios for lipids eluted from CD1 protein versus equivalently sized MHC proteins, which lack lipid-binding clefts.

(B) The total number of CD1-associated features was corrected to remove events with characteristics of false positive or redundant detection of isotopes, alternate adducts, and ion finding artifacts, yielding the number of unique events associated with each CD1 protein.

(C) Analysis of the linked and unlinked CD1 lipidomes yielded similar patterns for the number of ligands bound to each CD1 protein and similar percentages of lipids binding to 1, 2, 3, or 4 isoforms. Results in (A)–(C) are representative of two experiments for each protein set.

See also Figure S1 and Tables S1 and S2.

Cellular influence on capture

Capture outcomes are likely a function of at least three variables: the spectrum of lipids in each cell type, subcellular microenvironments that influence loading, and the constraints imposed by the shape of the four cleft types. We sought to understand or equalize variables related to endogenous lipid pools and subcellular trafficking so that lipid elution patterns might be linked to distinct cleft structures. To measure lipidomic overlap, we extracted total lipids from K562 and 293T cells to generate 4,163 total events , where 94% of total cellular lipids failed to meet change criteria (<5-fold, $p > 0.05$) (Figure 3A). The high lipidomic overlap in total cellular lipids helps to explain the similar patterns CD1 eluents in the two cell types (Figure 2).

Transmembrane truncation removed recycling motifs to allow normalized inter-isoform comparisons[48] but might also affect CD1 positioning within microenvironments in ways that affect antigen loading.[49] To allow CD1-lipid complex egress in a membrane-bound form, we engineered full-length CD1a and CD1b with human rhinovirus (HRV) 3C or tobacco etch virus (TEV) cleavage sites in the proximal extracellular domain, respectively.[24,50] This approach allows protease-mediated release of complexes at the surface (Figures 3B, 3C, and S3). After optimization of protease cleavage, we tested secreted versus normally trafficked but cleaved CD1a proteins (Figure 3B) for elution of SM and PC (SM/PC). This ratio is useful for quality control because it measures abundant sphingolipids and phospholipids, respectively, and they have similar MS response factors, so signal ratios correspond well to molar ratios.[47] We observed equivalent SM/PC ratios released from secreted and cleaved CD1a proteins (Figure 3B). For CD1b, stronger MS signals allowed more detailed profiling, showing that transmembrane tethering did not detectably skew profiles with regard to lipid class, chain length, or saturation (Figures 3C and 3D).

The apparent lack of influence of endosomal recycling was surprising because endosomal environments strongly influence exogenous lipid loading of CD1b.[18,21] Therefore, we further tested transmembrane tethering of CD1 in THP-1 cells, which more closely resemble professional antigen-presenting cells with active endocytosis pathways. Again, we found high lipodomic overlap of THP-1 and K562 cells and the lack of effect of tethering on PC and SM profiles (Figures 3A, 3C, and 3D). These results validated secreted proteins as a surrogate for transmembrane proteins by pointing away from dominant effects on lipid capture, a finding that matches recent results for CD1d.[25]

Annotating the CD1-lipidomes

To discover the molecular determinants of isoform-specific ligand capture, we needed to chemically identify molecules bound to multiple isoforms. Initially, MS signals were matched to published *m/z* values to preliminarily identify compounds. Then, compounds were compared with authentic standards (Figures 1D and 4A) in HPLC-MS and CID-MS analyses. For example, a PC-like molecule containing an ether-linked fatty acid (ether-PC [EPC]) yielded ions matching choline (*m/z* 104.108), phosphocholine (*m/z* 184.074), and a diacylglycerol with one ether-linked chain (*m/z* 563.540) that did not cleave with high energy (Figure 4B), as seen in the EPC standard (Figure S2J).

A third stage of analysis plotted features on *m/z* versus retention time axes to identify molecular variants of each solved molecule (Figure 4C). The keystone EPC nearly coeluted with 25 molecules varying in mass increments of 14.016 (CH2) and 2.016 (H2), corresponding to chain length and saturation variants, respectively. Similarly, the lead SM (*m/z* 813.684) whose lipid anchor contains 42 methylene units (CH2) with two unsaturations (42:2 SM) (Figure S2) appeared with 18 variants.

Overall, the linked CD1 lipidome reports 25 EPCs, 18 SMs, 10 ether-phosphatidylethanolamines PEs (EPEs), 2 ceramides (Cer), 16 SMs, 4 hexosylceramides, 5 dihexosylceramides, 3 deoxyceramides, 12 diacylglycerols, 5 triacylglycerols, 46 PCs, 4 lysophosphatidylcholines (LPCs), 15 PEs, and 3 lysophosphatidylethanolamines (LPEs) (Figures 4 and S2; Table S1). Separately, we identified 177 named lipids from unlinked CD1 lipidome (Table S2). In addition, 846 unique accurate mass values

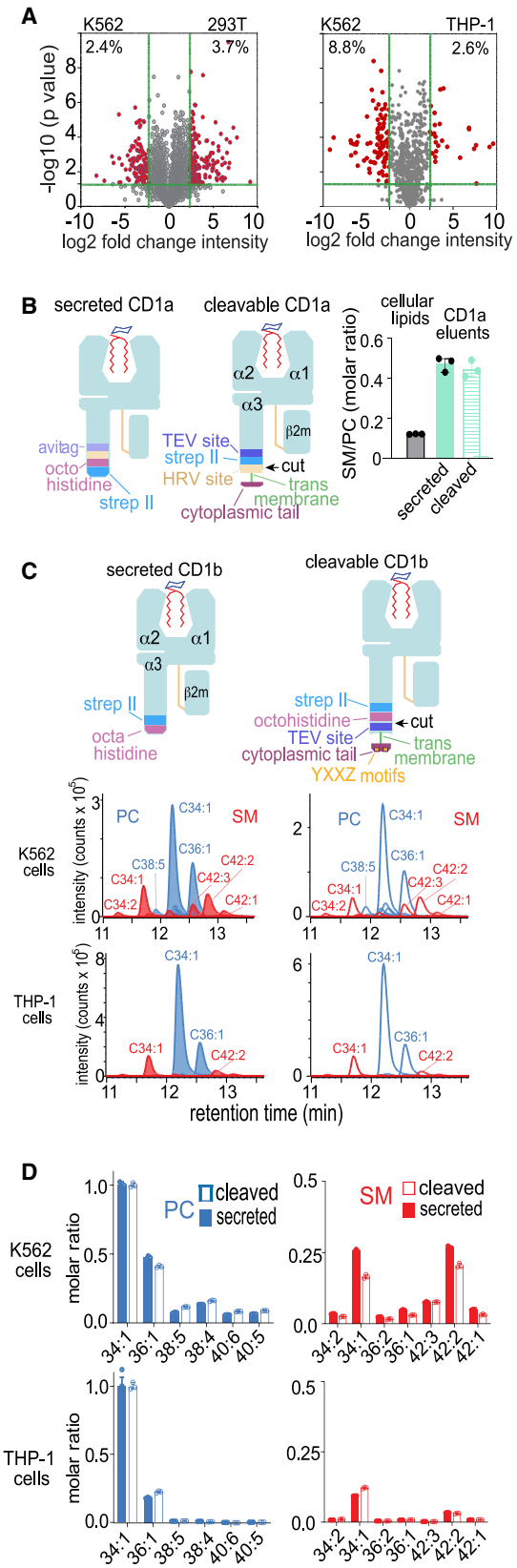

Figure 3. Influence of cell type and CD1 transmembrane tethering on lipidomic outcomes

(A) Total extracted lipids were compared to determine the percent lipidomic overlap by cell type.

(B) Cellular lipids were extracted in chloroform and methanol. CD1a proteins with a truncated transmembrane domain (secreted) were secreted into media. Transmembrane tethered CD1a was released into media by cleavage (cleaved) with human rhinovirus 3C protease. After being captured with nickel or streptactin, CD1a-eluted lipids were subjected to MS analysis to detect SM/PC ratios, showing that CD1a captures a higher ratio compared with cellular lipids as reported previously.[47]

(C and D) (C) CD1b proteins with intact transmembrane and cytoplasmic tail sequences encoding a four-residue tyrosine containing (YXXZ) motif that directs endosomal recycling in THP-1 cells and K562 cells were released by TEV protease and captured with nickel and streptactin, following by elution of lipids analyzed in comparison to a mass normalized preparation of secreted CD1b proteins. Eluted PCs and SMs (length: saturation) were detected as ion chromatograms (C) and quantitated by determining replicate chromogram areas (D). Results in (A)–(D) are representative of two experiments in each indicated cell type.

See also Figure S3 and Tables S1 and S2.

represent unnamed lipids that bind CD1 (Tables S1 and S2). Identifying lipids captured by multiple CD1 isoforms provided new biological insights. Ether-linked peroxisomal lipids are presented by CD1d to regulate NKT cell function,[51] and CD1a binds small lysolipids to free up the CD1 surface for direct TCR recognition.[52,53] Thus, finding EPCs, EPEs, LPC, and LPE in eluents from all CD1 isoforms points to broader roles of these ligands in the CD1 system (Figures 4B and 4D).

Emerging lipid length capture patterns

CD1 isoform-specific lipid capture motifs were unknown. CD1 genes are rarely polymorphic, so in humans, there are four clefts to consider: CD1a (1,280 Å^3), CD1b (2,200 Å^3), CD1c (1,780 Å^3), and CD1d (1,650 Å^3), which differ in shape and size.[10–13] Previously known antigens and the 327 named trans-CD1 isoform ligands detected here (Figure 4) possess chemical variables in their lipid anchors that could govern binding. Therefore, we compared all lipid signals from all four CD1 isoforms to seek isoform-specific pairing with named lipids. Principal components analysis showed clear clustering of lipid intensity patterns as a function of CD1 isoform in both lipidomes, supporting the existence of isoform-specific capture motifs (Figure 5A).

Differential abundance analysis identified capture patterns based on CD1 isoform, lipid head groups, lipid anchor type, unsaturation, and chain length. Although the analysis was unsupervised, lipids with similar structures showed similar patterns of CD1 isoform specificity, suggesting structurally based interactions of CD1 proteins with lipid anchors. For example, PCs with the shortest chains (C30–C38) skewed to CD1b, intermediate PCs (C38–C40) skewed to CD1a, and long-chain PCs (C42–C46) skewed to CD1d (Figure 5B). By contrast, CD1c showed equivalent capture across the full-length range found in cells (C30–C46). Notably, these chain length-based capture patterns (CD1b < CD1a < CD1d) were different from the hierarchy of cleft volumes (CD1a < CD1d < CD1c < CD1b). However, the patterns were likely valid, as length-based PC capture patterns were seen in both the linked and unlinked datasets, and they were recapitulated in other phospholipid families, including PE, EPC, and

Please cite this article in press as: Huang et al., CD1 lipidomes reveal lipid-binding motifs and size-based antigen-display mechanisms, Cell (2023), https://doi.org/10.1016/j.cell.2023.08.022

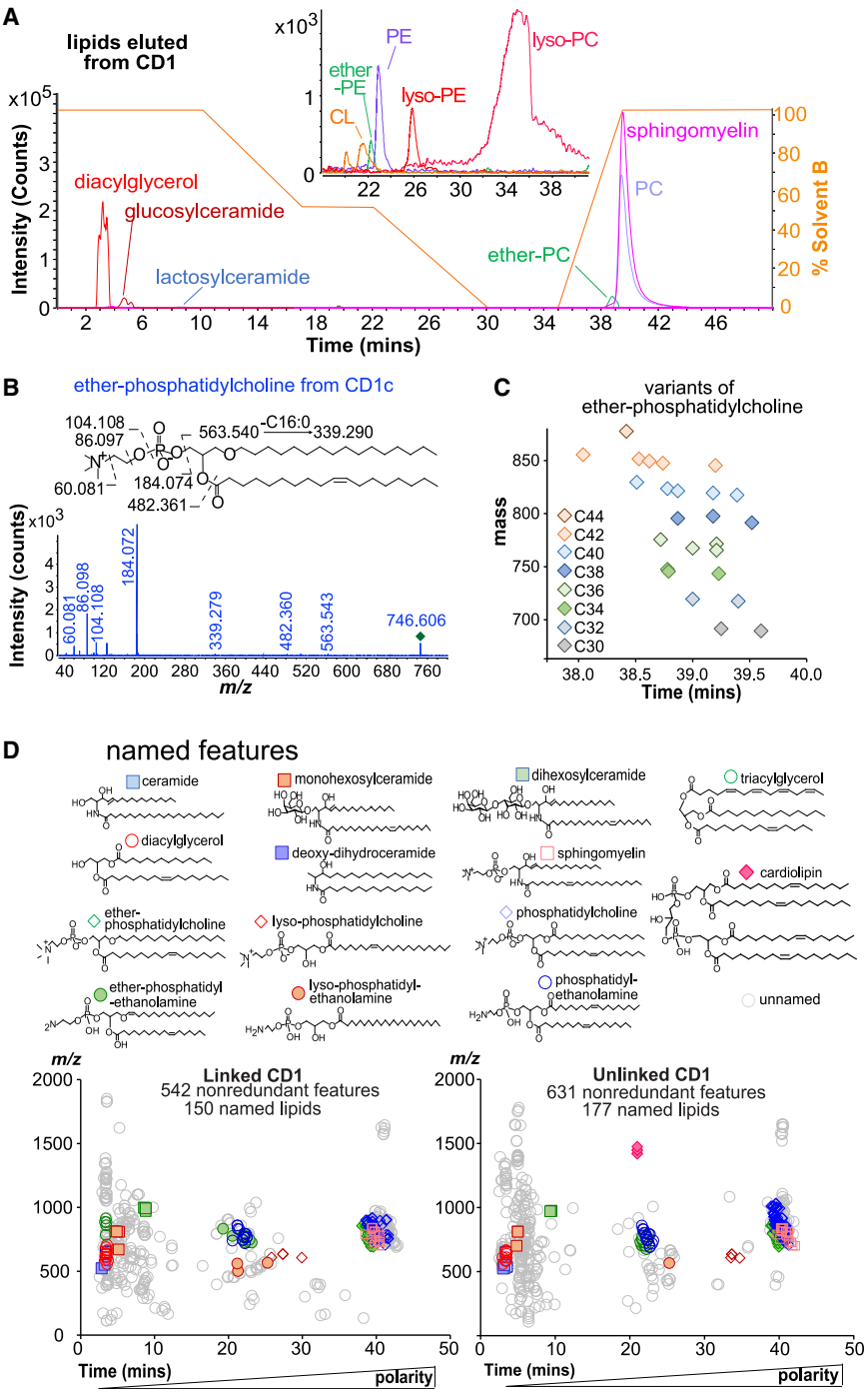

Figure 4. Annotating compounds binding to all four human CD1 isoforms

(A) The indicated chemical assignments derive from co-elution with standards (Figure 1D) and matching detected mass values to diacylglycerol (*m/z* 612.557), triacylglycerol (*m/z* 812.691), hexosylceramide (*m/z* 810.681), dihexosylceramide (*m/z* 972.734), cardiolipin (CL, *m/z* 1,419.002), ether-phosphatidylethanolamine (EPE, *m/z* 728.557), PE (*m/z* 768.552), lysophosphatidylethanolamine (LPE, *m/z* 566.416), lysoPC (LPC, *m/z* 608.465), EPC (*m/z* 746.606), PC (*m/z* 760.585), or SM (*m/z* 813.685), as well as CID-MS that detected diagnostic fragments (Figure S2).

(B) For example, the unknown at *m/z* 746.622 matched the mass of an ether-PC, and CID revealed neutral loss of phosphatidylcholine (*m/z* 563.540) and C16 or C18:1 fatty acyl units (*m/z* 339.279, 482.360).

(C) Plotting events yields clusters, where recognizable mass intervals identified 25 EPCs with the indicated total chain length (colors), with varied saturation that influences retention.

(D) Repeating this process, clusters were solved as the indicated molecules, where unsaturation positions are inferred.

See also Tables S1 and S2.

EPE (Figure 5B). Furthermore, SMs mirrored key patterns seen for phospholipids, showing the least distinct length optima for CD1c and the shortest length for CD1b binding (C34–C36). Although fewer lipids varied only in saturation, among C40–C42 PCs, polyunsaturation correlated with less capture by CD1d and increased capture by CD1b (Figure 5B). In summary, these length patterns were unexpected because CD1b had the largest cleft volume, yet consistently bound shorter lipids.

Cellular editing of the endogenous lipidome

Lipid "editing" describes active cellular processes that promote or block lipid exchange onto CD1 proteins to influence responses to certain lipids or to lipids present in certain subcellular locations.[54] To broadly measure editing, we first generated lipidomes for total lipids from K562 and 293T cells as a measure of each lipid's background level and then aligned the signals with eluents from CD1 proteins in the same cell type. Notably, we found many matching signals in the cellular lipid and CD1 eluents (Figure 5C), indicating that unlike chemically processed peptides for T cells, many self-lipids are presented in an unmodified form. Although all CD1 isoforms detectably bound many abundant cellular lipids (Figures 2C and 5B) and some capture ratios were near 1 (Figure 5C), many diverged strongly (2-fold to 5,000-fold) from background levels, suggesting that cells actively influence which lipids are displayed. Certain patterns might derive from general cellular effects or experimental artifacts. For example, parallel changes for the same lipid with all four isoforms might appear for any lipid that is overexpressed in the secretory pathway. Also, long-chain lipids might be better retained on all CD1 isoforms during protein purification. However, neither pattern was widespread. Most lipids showed complex patterns of isoform-specific overcapture

Please cite this article in press as: Huang et al., CD1 lipidomes reveal lipid-binding motifs and size-based antigen-display mechanisms, Cell (2023), https://doi.org/10.1016/j.cell.2023.08.022

CellPress
OPEN ACCESS

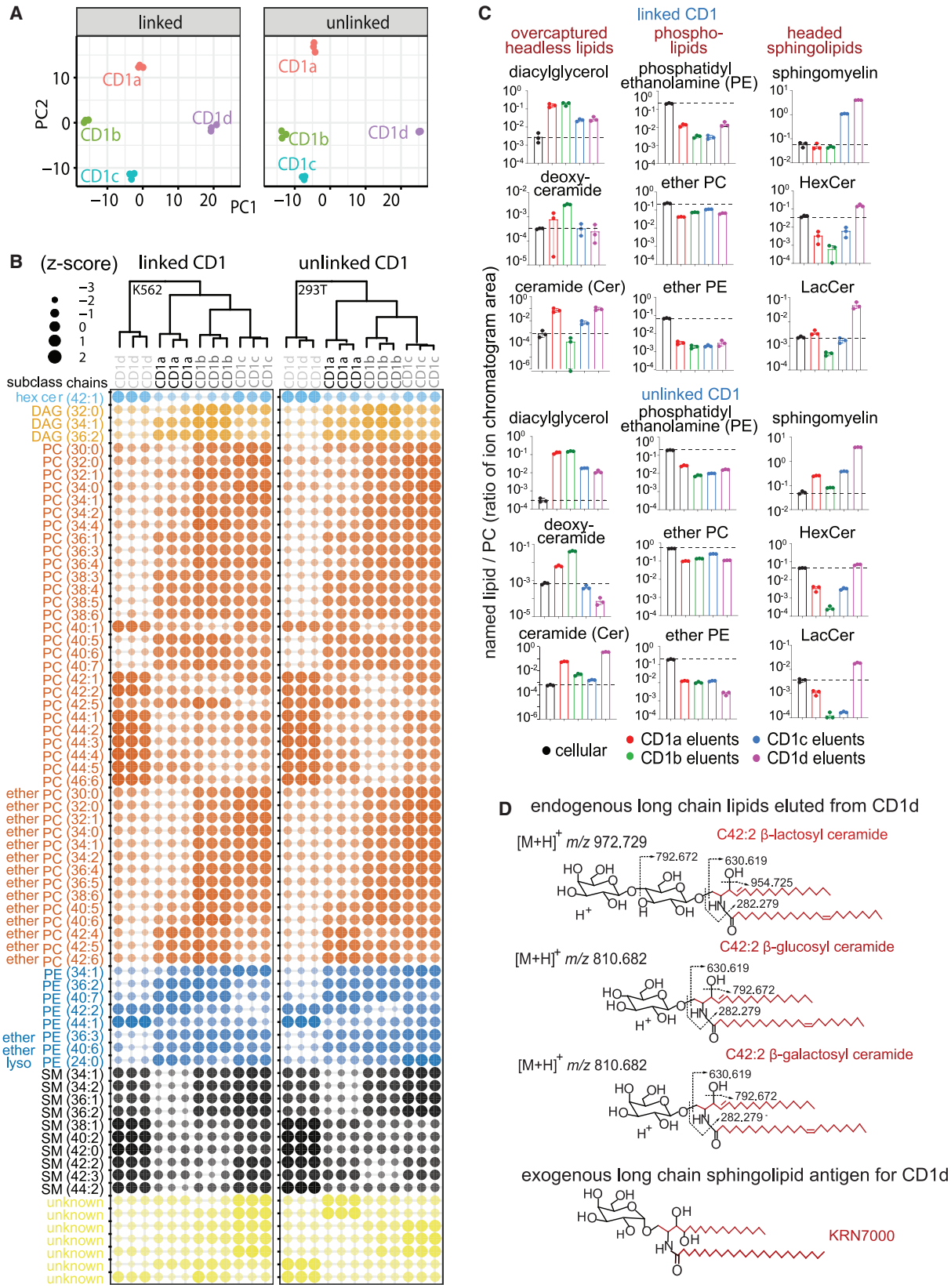

(legend on next page)

Please cite this article in press as: Huang et al., CD1 lipidomes reveal lipid-binding motifs and size-based antigen-display mechanisms, Cell (2023), https://doi.org/10.1016/j.cell.2023.08.022

by lipid class (Figure 5C) and length (Figure S4), suggesting differential cleft-specific interactions.

Strikingly, both mono- and di-hexosyl ceramides showed strong capture by CD1d but lower capture by other isoforms in both lipidomes and both analyses (Figures 5B, light blue, and 5C, pink). The clear CD1d-specific capture could be immunologically significant because synthetic hexosylceramide superagonists[6,55] and bacterial antigens[56,57] have dominated research on CD1d and NKT cells; however, self-cellular sphingoglycolipids were proposed as NKT regulators[58] but have not been clearly biochemically detected in cells. Therefore, we undertook further HPLC-MS and CID-MS analysis of hexosyl ceramides to determine their complete structures as β-glucosylceramide, β-galactosylceramide, and lactosylceramide (Figures 5D, S2K, and S2L). The apparent CD1d-specific sphingolipid capture motif extends the known relationship of CD1d, previously based on foreign hexosyl-ceramides, to now involve self-glycosphingolipids, providing new candidate molecules for control of tissue-resident NKT cells during sterile inflammation.[59,60]

Also, a major new hypothesis is that SMs are natural blockers of CD1d-[25,61] and CD1a-mediated[47] T cell responses. Indeed, CD1d showed uniquely high SM overcapture ratios of in excess of 100-fold, suggesting that high intrinsic SM capture could contribute to the blockade of NKT cells seen *in vitro* and *in vivo*.[25,61] Long-chain SM also blocks T cell recognition of CD1a[47], but CD1a overcapture of total SM was modest and varied (Figure 5C). However, focused analysis based on chain length showed that only long-chain (C42) SM was overcaptured by CD1a in cells (Figure S4), confirming the prior report.[47] Long-chain length also correlated with better capture of other sphingolipids by CD1d, similar to patterns observed for foreign α-galactosyl ceramides.[55] Finally, another general pattern is under-capture of phospholipids (PE, EPE, and EPC) by all CD1 isoforms. However, their high absolute abundance in cells allows them to generate intermediate signals in CD1 eluents (Figure 5C). Overall, patterns from overcapture analysis reproduced in both lipidomes (Figure 5C) and enrichment analysis (Figure 5B), providing a four-way validation as emergent CD1 lipid-binding motifs.

Matches and mismatches of lipid length to cleft volume

Compared with MHC grooves, CD1 clefts surround their ligands more extensively, supporting the expectation that cleft volume might match ligand size. However, CD1b has a particularly large cleft volume[10] but captured ligands with similar overall average mass compared with other isoforms (Figure 6A; Tables S1 and S2). Considering named lipids, where lipid anchor size is explicitly known (Figures 5B, 5C, and S4), CD1b captured PCs and sphingolipids (C30–C36) at the low end of the length spectrum in cells (C30–C48). CD1b ligands showed shorter lipid tails than those in ligands captured by the smaller clefts in CD1a (C36–C40) and CD1d (C38–C46). To investigate this size mismatch further, we revisited CD1 cleft volume measurements.

We reanalyzed the four earliest solved structures that originally defined cleft volumes for each isoform,[10–13] along with 54 subsequently solved structures (Table S3) and 5 structures reported here. Using one uniform method with Connolly solvent-excluded calculations[62] and a probe radius of 1.7 Å (Figures 6B and 6C), volume variance informed structural flexibility as being higher for CD1c than other isoforms (Figure S5). The CD1b volume estimate was not changed, but CD1a, CD1d, and CD1c[42,63,64] were revised upward: CD1b (2,220 $Å^3$) > CD1c (2,060 $Å^3$) > CD1d (1,760 $Å^3$) ~ CD1a (1,690 $Å^3$).

Next, guided by crystal structures generated through exogenous lipid loading (Table S3), we determined the number of CH2 units inside clefts (Figures 6B and 6C). CD1a bound ligands with a mean of C38.3 for two-tailed lipids or C16.7 for single-tailed lipids (range C15–C42). The size of ligands in CD1d (mean C38.8, range C33–C42), CD1c (mean C47.3, range C32–C60), and CD1b (65.1, range C50–C85) differed substantially. Combined, these measurements of mean lipid anchor size (Figures 5B, 5C, and 6A) and mean cleft volume (Figures 6B and S5) led to emergent size motifs. For CD1a and CD1d, anchors in eluted lipids (~C38) matched cleft volumes (C38.3–C38.8). CD1c ligands were longer and more variable, correlating with greater structural flexibility of the CD1c protein. For CD1b, cleft volume and lipid ligand length showed extreme and apparently universal mismatch: CD1b is larger than CD1a and CD1d by ~500 $Å^3$ or ~27 CH2, but the eluted lipids were smaller. The length disparity between ligands (~C30–C36) and cleft size (~C65) supported an alternative hypothesis: CD1b normally binds two small self-lipid ligands.

Crystallography of CD1b with endogenous lipids

Dual lipid binding was indirectly supported by prior CD1b structures of refolded[10] and native[65] CD1b. However, a limitation of prior crystallographic sizing (Figure S5) was that ligands were chosen and loaded exogenously as pure molecules in cell-free conditions, but cellular capture involves loading from a pool of diverse endogenous self-lipids. Therefore, we considered an unconventional approach of bypassing the loading of named ligands. Instead, we directly solved untreated CD1b proteins carrying endogenous lipids (CD1b-endo). A high-resolution structure (Figure 7A; Table S4) showed that the head group density corresponded best to PC (Figure 7A), correlating to high signals for PC from the lipidome (Figures 4 and 5B). One C40 lipid

Figure 5. Chemical determinants of capture by individual CD1 isoforms

(A) Principal components analysis of differentially abundant lipids (Benjamini-Hochberg adjusted $p < 0.05$ based on F-statistic) determines lipid patterns released from linked (K562 cells) or unlinked (293T cells) CD1 proteins.

(B) Bubble plot of 70 lipids with significantly different abundance (adjusted $p < 0.05$) showed isoform-specific capture of lipids based on lipid subclass, length, and saturation.

(C) After normalizing signal intensity for each named lipid to total PC, named lipids in eluents from each CD1 protein are reported versus total lipid signal (dotted line) as the background value.

(D) After initial studies detected mono- and di-hexosyl ceramides, their identification as β-glucosyl ceramide, β-galactosyl ceramide, and lactosyl ceramide was accomplished based on co-elution with standards and the indicated CID-MS fragments (Figures S2K and S2L). CD1d-specific binding of three long-chain self-sphingolipids identified here have anchors (red) that chemically resemble known foreign long glycolipids presented by CD1d.

See also Figure S4.

Please cite this article in press as: Huang et al., CD1 lipidomes reveal lipid-binding motifs and size-based antigen-display mechanisms, Cell (2023), https://doi.org/10.1016/j.cell.2023.08.022

A

		CD1a	CD1b	CD1c	CD1d
mean m/z	**linked CD1**	735	744	736	721
	unlinked CD1	779	790	795	788

B

	Structures	15	20	8	>20
Volume ($Å^3$)	first solved	1280	2200	1780	1650
	consensus (mean ± S.D.)	**1690 ± 180**	**2220 ± 110**	**2060 ± 220**	**1760 ± 150**
Methylene Unit Count (C)	antigenic lipids	one tail: 16.7 two tail: 38.3	34.9	28.3	37.1
	spacer/ scaffold lipids	not seen	32.1	21.7	rarely seen
	total	**one tail: 16.7 two tail: 38.3**	**65.3**	**47.3**	**38.8**

C

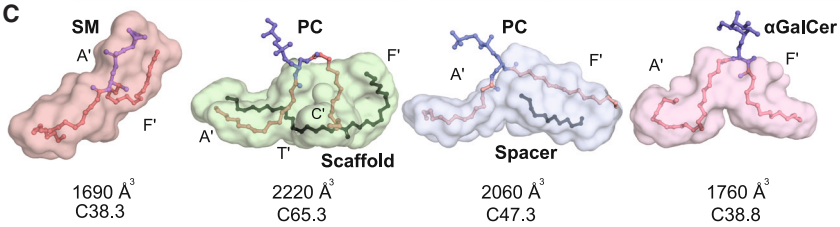

Figure 6. Measurements of CD1 cleft volume

(A) Mean *m/z* values of lipids eluted from each CD1 isoform are shown.

(B and C) Volume ($Å^3$) calculations for the first solved structures of each human isoform were reported using differing modeling assumptions. Consensus values derive from reanalyzing these four structures and 59 subsequently solved structurs with a uniform method (Table S3). The mean number of methylene units (CH2) was calculated in structures with single or double-tailed antigens (CD1a) and with the combined size of antigens, spacer, and scaffold lipids (CD1b, CD1c, and CD1d). Cleft surface traces depict the volume ($Å^3$), as well as the number of methylene units in lipid tails within each type of CD1cleft. See also Figure S5 and Tables S3 and S4.

resided in the upper portion of the cleft, and a second, nearly linear C16 density was positionedbeneath, directly supporting the dual ligand model.

To further assess lipid positioning, CD1b-endo complexes were treated with lipids that match the chemical structures of endogenous CD1b ligands detected in eluents (Figures 4 and 5). We solved CD1b with C34 PE (1.6 Å), C34 SM (2.0 Å), and lysosulfatide (1.9 Å). Similar to CD1b-endo, these three hybrid structures showed two distinct densities (Figure 7B). Overlay showed strikingly conserved positioning of both densities, except for small size differences near T′-F′ junction (Figure 7C). The dual chain antigens, PE and SM, resided in the upper chamber in the A′ and C′ pockets. The single chain of lysosulfatide was in the A′ pocket, whereas an ethylene glycol from buffer was in the C′ pocket. No significant contacts with CD1b are observed for the PC and PE headgroups (Figures 6A and 6B),[66,67] but for SM, bonds with Gln152 were noted (Figure S6C). The lysosulfatide headgroup spans across to the F′ portal, forming a hydrogen bond with Thr157 (Figure S6D; Table S5).

Lipid seating defines functional chambers within CD1b

In all cases, "antigenic lipids" lie in the upper section of the CD1b cleft, and a separate linear density lies near the bottom of the cleft (Figures 7A–7D). These small linear densities are likely endogenous "scaffold lipids" derived from the cellular expression system. Their deep seating suggests that they prop up antigenic lipids for contact with TCRs but cannot themselves contact TCRs. Importantly, all four structures demonstrated a 1:1:1 stoichiometry of CD1b:antigen:scaffold. Densities did not take random positions but instead showed two defined positions that represent upper and lower chambers (Figure 7D). CD1b contrasts with CD1c, where spacer lipids can be sometimes present but differ in size and position in structures solved to date (Figure S7). Combined, the two densities in CD1b have a length of C56–C65 (Figure 7C) that matches the estimated cleft volume capacity (~C65) (Figure 6C), so 2:1 stoichiometry potentially explains the size discrepancy between eluted ligands and the cleft.

Two-step modular model of lipid exchange

The two-chamber model might also explain a longstanding observation, whereby CD1b can readily load short (~C32) glucose monomycolate (GMM) antigens, but long-chain (~C76–C86) antigens require recycling of CD1b proteins into the endolysosomal pathway.[21] A revised model, based on our findings, is that small (~C32) exogenous antigens displace one endogenous lipid in the upper chamber, but large (~C80–C86) lipid loading requires ejection of both endogenous lipids. Extending a prior study,[68] we synthesized C85 GMM[69] and co-crystallized it with CD1b to test the positioning of very long-chain mycolates. The resolved electron density revealed the (C59) meromycolate tail spanning the A′ T′ F′ channel, with the (C26) α-branch in the C′ pocket (Figure 7E). Only 17 carbons of the α-branch were visible inside CD1b, suggesting that the terminal C9 unit protrudes from the C′ portal. This structure demonstrated the ejection of both self-lipids. Also, the much larger exogenous lipid traced a highly similar path compared with the two self-lipids. Finally, these outcomes point to mechanisms for accommodating lipids with varying sizes. Longer lipids curve upward from the T′ tunnel into the F′ pocket. For the largest C85 antigen, the α-branch likely protruded to the outer surface through the C′ portal.

DISCUSSION

Measurements of 63 CD1 cleft volumes, ~4,000 trackable CD1 ligand addresses, and ~160 named molecules address basic

Please cite this article in press as: Huang et al., CD1 lipidomes reveal lipid-binding motifs and size-based antigen-display mechanisms, Cell (2023), https://doi.org/10.1016/j.cell.2023.08.022

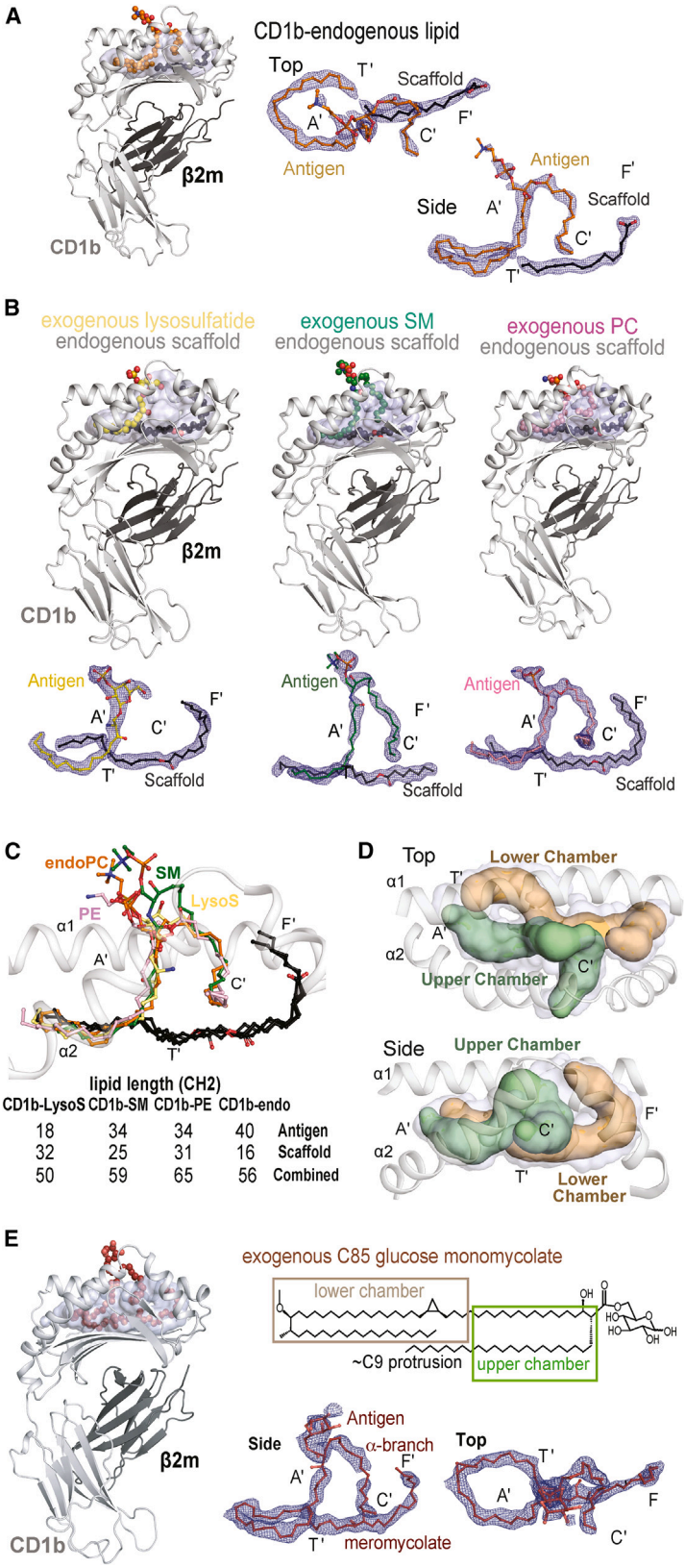

Figure 7. Upper and lower chambers of CD1b

(A) Structural overviews of CD1b carrying endogenous lipids (CD1b-endo) show densities corresponding to the antigenic (orange) and a scaffold lipid (black).

(B) CD1b-endo complexes were treated with SM (green), phosphatidylethanolamine (pink), or lysosulfatide (yellow). Electron density maps (contoured to 0.9 σ) demonstrate seating of antigenic (colored) lipids in the upper chamber that overlap with the A′ and C′ pockets, whereas scaffold lipids reside in the lower chamber that overlaps with the T′ and F′ pockets.

(C) Overlay of CD1b-endo complexes, including those treated with exogenous antigens, shows similar positioning of antigens (colors) and scaffolds (black). For exogenous lipids, chain lengths were known from the molecules added, which also matched the size of the observed density.

(D) The upper chamber (green) holds the antigenic lipid, and the lower chamber (brown) contains the scaffold lipid.

(E) CD1b solved in complex with C85 GMM, which contains a C26 α-branch and a C59 meromycolate chain. The density corresponds to a C76 lipid, suggesting that the α-branch protrudes (C9 protrusion). Viewed from above, the meromycolate chain threads clockwise in the A′ pocket and couterclockwise in the A′-T′ junction. The path of the exogenous mycolate lipid (E) is similar to the threaded position of two self-lipids seen in CD1b-endo and CD1b-antigen structures in (B) and (C).

See also Figures S6 and S7 and Tables S2 and S3.

questions regarding the cellular lipid display to T cells. The four partially overlapping lipidomes from the human CD1 isoforms document a display of at least 1,300 unique lipids, which represents a broad coverage of self-cellular lipids. Overcapture analysis compared cellular with CD1-bound lipids, finding many matches, suggesting that lipids are frequently presented in a chemically unmodified form.[70] Thus, unlike peptide antigen processing for T cells, which nearly universally requires trimming of proteins down to size, the CD1 system likely solves size issues through specialized seating mechanisms and altered stoichiometry of CD1:lipid. Lipidomics and crystallography support that each CD1 isoform shows distinct patterns of overcapture of certain lipids. We propose three general capture mechanisms that depend on whether clefts match (CD1a, CD1d), partially match (CD1c), or universally mismatch (CD1b) lipid anchor size.

Self-ligands eluted from CD1a and CD1d show optimal anchor length of C38, which matches measured cleft volumes for CD1a (1,690 Å^3) and CD1d (1,760 Å^3) and calculated cleft capacities of C38.3 or C38.8. This size match, low volume variance among 48 crystal structures, and the lack of spacer lipids in most crystal structures all point to 1:1 CD1:lipid stoichiometry as the usual cellular mechanism of endogenous lipid capture. Furthermore, CD1a and CD1d eluents co-clustered in unsupervised enrichment analysis, and both showed preferential capture of sphingolipids over phospholipids. The key difference is that sphingolipid overcapture was stronger for CD1d and occurred independently of chain length, whereas CD1a overcapture required very long (>C36) chain sphingolipids. The sphingolipid-specific overcapture patternfor CD1d involves at least five endogenous sphingolipids: SM, ceramides, glucosylceramides, galactosylceramides, and lactosylceramides. The concordant patterns seen in both lipidomes and analyses could explain how self-sphingolipids, acting alongside the known roles of foreign long-chain sphingoglycolipids, could be enriched on cellular CD1d to influence T cell response. Whereas CD1 ligands are usually considered in terms of antigenic potential, SMs inhibit T cell responses, so their high rate of capture by CD1d and CD1a could support the dominant negative blocking effects seen *in vitro*[25,47] and *in vivo*.[61]

CD1c was known to have structural flexibility near the antigen entry portal,[12,63] and our analysis found high cleft volume variance. This flexibility matches patterns seen in eluted lipids: PC and SM subspecies were highly variable (C30–C46), and unlike other isoforms, they showed no clear length optimum. The mean lipid anchor size (C39) is smaller than the predicted cleft volume (C47.3), but the large ligand size range (C32–C60) excluded a fundamental size discrepancy with cleft volume. Consistent with this partial size mismatch, only some CD1c-lipid structures showed spacer lipids, which, unlike the precisely positioned scaffold lipids in CD1b, were of markedly differing size and positioning. Thus, the CD1c self-lipid motif is less predictive, but can be articulated: one antigenic lipid with higher length variability (C30–C46) and occasional use of diversely positioned spacer lipids.

For CD1b, cleft capacity (~C65, 2,220 Å^3) showed essentially no overlap with the size of eluted lipid anchors (C30–C42). This nearly universal, ~2-fold mismatch provided broad evidence for dual ligand capture, which was validated by four CD1b structures showing 2:1 lipid:CD1b stoichiometry with strikingly reproducible positioning. Lipids coil nearly 360° within the A′ pocket and take a sharp turn at the A′-T′ junction so that the final lipid positioning is similar, despite the differing number of lipids loaded (1 or 2) or their origin from endogenous versus exogenous sources. Lipid positioning outcomes were similar in proteins refolded outside of cells,[10] suggesting that the CD1b heavy chain itself has an intrinsic, but not yet understood, threading mechanism to precisely seat complex lipids. Whereas CD1 'pocket' nomenclature is usually defined by protein landmarks, the relatively uniform seating of two lipids can define functional upper and lower 'chambers' in CD1b.

Given the lack of detected self-ligands with >C65 chain length and uniform seating patterns in CD1b-endo crystal structures, we propose not merely that dual lipid capture occurs[10,65] but that it is the usual mechanism of self-lipid capture by CD1b in cells. Early studies identified large (C76–C86) foreign ligands for CD1b,[3,71,72] but even sensitive MS experiments reported here failed to detect comparatively large endogenous placeholders. Instead, our data suggest that the placeholder function is normally subsumed by two self-lipids. The ready loading of small lipids[21,73] required the expulsion of one placeholder in the upper chamber, whereas large exogenous GMM lipids must replace both. Crystal structures shown here capture all key intermediates predicted by this two-stage exchange model: two small endogenous lipids, one small endogenousalongside one small exogenous lipid, as well as one large exogenous lipid.

Given the distinct architecture of each isoform, finding that half of all CD1 ligands bind all four human CD1 antigen-presenting molecule types was unexpected. Individual TCRs do not recognize the same antigen presented by two CD1 proteins. Therefore, these isoform-overlap patterns suggest broad immunosurveillance but not degenerate T cell response to CD1-lipid pairs. However, there are limits to the flexibility of capture, since nearly half of all lipids did not detectably bind all isoforms. Also, each isoform showed preferences based on lipid class and chain length. The diversity of lipids displayed points to broad lipid recognition, rather than evolution driven by any single-dominant lipid, like α-hexosyl ceramides. This comprehensive listing of ~1,300 unnamed CD1 ligands of known mass likely contains molecular addresses of molecules that are yet to be discovered as antigens and TCR-blocking lipids. Thus, the CD1 lipidomes provide a comprehensive resource of both named and unnamed lipids for any investigator to match CD1-displayed lipids with new immunogenic or regulatory lipids as they are discovered in other fields of research.

Limitations of the study

This study focused on the secretory pathway, where all CD1 isoforms have similar trafficking. Unexpectedly, our studies of CD1b and recent studies of CD1d[25] failed to detect the strong effects of CD1 recycling on self-lipid capture. One limitation is that the scope of lipidomic measurements for recycled proteins released with proteases is limited to major sphingolipids and phospholipids. Also, proteases likely cleave both pre- and post-endosomal CD1b proteins, so we do not rule out that future studies of pure post-endosomal proteins could detect CD1 recycling-dependent lipid capture patterns. Another limitation is that

length and other chemical motifs describe the usual self-lipids captured by CD1 proteins but not universal capture patterns. Rare ligands that do not match motifs are seen in the lipidome, and they could influence T cell response.

STAR★METHODS

Detailed methods are provided in the online version of this paper and include the following:

- KEY RESOURCES TABLE
- RESOURCE AVAILABILITY
  - Lead contact
  - Materials availability
- EXPERIMENTAL MODEL AND STUDY PARTICIPANT DETAILS
  - Human cell culture
- METHOD DETAILS
  - CD1 and MHC expression
  - Mass spectrometry-based comparative lipidomics
  - Lipidomic analyses
  - Chemical annotation of molecular features
  - Determination of media lipid binding
  - Structural characterization of CD1b presenting SM, lysosulfatide, PE, endogenous PC, and GMM C85
  - Consensus cleft volume calculations
- QUANTIFICATION AND STATISTICAL ANALYSIS

SUPPLEMENTAL INFORMATION

Supplemental information can be found online at https://doi.org/10.1016/j.cell.2023.08.022.

ACKNOWLEDGMENTS

This work was supported by the NIH (AR048632, AI115358, and 75N93020D00005), the Wellcome Trust Collaborative Award (209222/Z/17/Z), the American Lung Association (IA-629987), NHMRC (1128924, 1159272, and 2008981), the ARC (DE210101031), the Chinese Academy of Medical Sciences Innovation Fund for Medical Science (2018-I2M-2-002), the UK Medical Research Council, and the UKRI (MC_UU_00008). For open access, the authors applied a CC BY public copyright license to any Author Accepted Manuscript version arising from this submission. We thank Gina Bia, Lixia Han, Kelly Jeter, Kyla Ugwu, Vasanthi Govindu, Rick Willis, John Shires, and Dale Long for protein production.

AUTHOR CONTRIBUTIONS

The study was initiated by S.H. and D.B.M. with structural validations designed by J.R. Protein expression, lipid elution, and MS analyses were designed and performed by S.H., T.-Y.C., G.S.O., C.S.H., Y.-L.C., S.W.N., and J.D.A. T.Y.C. and S.H. annotated lipids. Co-crystals and cleft modeling were carried out by A.S., R.F., G.R.B., and S.G. J.A.M. provided bioinformatic analysis. A.J.M. and N.T. synthesized mycolyl lipids. The manuscript was written by S.H., J.R., and D.B.M. with input from all authors.

DECLARATION OF INTERESTS

The authors hold intellectual property through the Massachusetts General Brigham (D.B.M., G.S.O., and J.R.; filing 29618-0390P01) and the University of Oxford (G.S.O., C.S.H., and Y.-L.C.; filings 2116709.3, 2217923.8, 2217924.6). G.S.O. collaborates with UCB and Janssen, and D.B.M. consults for Pfizer.

INCLUSION AND DIVERSITY

We support inclusive, diverse, and equitable conduct of research.

Received: September 16, 2021
Revised: May 5, 2023
Accepted: August 21, 2023
Published: September 18, 2023

REFERENCES

1. Garboczi, D.N., Ghosh, P., Utz, U., Fan, Q.R., Biddison, W.E., Wiley, and D C. (1996). Structure of the complex between human T-cell receptor, viral peptide and HLA-A2. Nature *384*, 134–141.
2. Garcia, K.C., Degano, M., Stanfield, R.L., Brunmark, A., Jackson, M.R., Peterson, P.A., Teyton, L., and Wilson, I.A. (1996). An alphabeta T cell receptor structure at 2.5 A and its orientation in the TCR-MHC complex. Science *274*, 209–219.
3. Beckman, E.M., Porcelli, S.A., Morita, C.T., Behar, S.M., Furlong, S.T., and Brenner, M.B. (1994). Recognition of a lipid antigen by CD1-restricted alpha beta T cells. Nature *372*, 691–694.
4. Zeng, Z., Castaño, A.R., Segelke, B.W., Stura, E.A., Peterson, P.A., and Wilson, I.A. (1997). Crystal structure of mouse CD1: an MHC-like fold with a large hydrophobic binding groove. Science *277*, 339–345.
5. Fowlkes, B.J., Kruisbeek, A.M., Ton-That, H., Weston, M.A., Coligan, J.E., Schwartz, R.H., and Pardoll, D.M. (1987). A novel population of T-cell receptor alpha beta-bearing thymocytes which predominantly expresses a single V beta gene family. Nature *329*, 251–254.
6. Kawano, T., Cui, J., Koezuka, Y., Toura, I., Kaneko, Y., Motoki, K., Ueno, H., Nakagawa, R., Sato, H., Kondo, E., et al. (1997). CD1d-restricted and TCR-mediated activation of Valpha 14 NKT cells by glycosylceramides. Science *278*, 1626–1629.
7. Bendelac, A., Lantz, O., Quimby, M.E., Yewdell, J.W., Bennink, J.R., and Brutkiewicz, R.R. (1995). CD1 recognition by mouse NK1+ T lymphocytes. Science *268*, 863–865.
8. Van Rhijn, I., Godfrey, D.I., Rossjohn, J., and Moody, D.B. (2015). Lipid and small-molecule display by CD1 and MR1. Nat. Rev. Immunol. *15*, 643–654. https://doi.org/10.1038/nri3889.
9. de la Salle, H., Mariotti, S., Angenieux, C., Gilleron, M., Garcia-Alles, L.F., Malm, D., Berg, T., Paoletti, S., Maître, B., Mourey, L., et al. (2005). Assistance of microbial glycolipid antigen processing by CD1e. Science *310*, 1321–1324.
10. Gadola, S.D., Zaccai, N.R., Harlos, K., Shepherd, D., Castro-Palomino, J.C., Ritter, G., Schmidt, R.R., Jones, E.Y., and Cerundolo, V. (2002). Structure of human CD1b with bound ligands at 2.3 A, a maze for alkyl chains. Nat. Immunol. *3*, 721–726.
11. Zajonc, D.M., Elsliger, M.A., Teyton, L., and Wilson, I.A. (2003). Crystal structure of CD1a in complex with a sulfatide self antigen at a resolution of 2.15 A. Nat. Immunol. *4*, 808–815.
12. Scharf, L., Li, N.S., Hawk, A.J., Garzón, D., Zhang, T., Fox, L.M., Kazen, A.R., Shah, S., Haddadian, E.J., Gumperz, J.E., et al. (2010). The 2.5 a structure of CD1c in complex with a mycobacterial lipid reveals an open groove ideally suited for diverse antigen presentation. Immunity *33*, 853–862. https://doi.org/10.1016/j.immuni.2010.11.026.
13. Koch, M., Stronge, V.S., Shepherd, D., Gadola, S.D., Mathew, B., Ritter, G., Fersht, A.R., Besra, G.S., Schmidt, R.R., Jones, E.Y., and Cerundolo, V. (2005). The crystal structure of human CD1d with and without alpha-galactosylceramide. Nat. Immunol. *6*, 819–826.
14. Borg, N.A., Wun, K.S., Kjer-Nielsen, L., Wilce, M.C.J., Pellicci, D.G., Koh, R., Besra, G.S., Bharadwaj, M., Godfrey, D.I., McCluskey, J., and Rossjohn, J. (2007). CD1d-lipid-antigen recognition by the semi-invariant NKT T-cell receptor. Nature *448*, 44–49.

15. McMichael, A.J., Pilch, J.R., Galfré, G., Mason, D.Y., Fabre, J.W., and Milstein, C. (1979). A human thymocyte antigen defined by a hybrid myeloma monoclonal antibody. Eur. J. Immunol. *9*, 205–210.

16. Kang, S.-J., and Cresswell, P. (2002). Regulation of intracellular trafficking of human CD1d by association with MHC class II molecules. EMBO J. *21*, 1650–1660.

17. Briken, V., Jackman, R.M., Dasgupta, S., Hoening, S., and Porcelli, S.A. (2002). Intracellular trafficking pathway of newly synthesized CD1b molecules. EMBO J. *21*, 825–834.

18. Jackman, R.M., Stenger, S., Lee, A., Moody, D.B., Rogers, R.A., Niazi, K.R., Sugita, M., Modlin, R.L., Peters, P.J., and Porcelli, S.A. (1998). The tyrosine-containing cytoplasmic tail of CD1b is essential for its efficient presentation of bacterial lipid antigens. Immunity *8*, 341–351.

19. Briken, V., Jackman, R.M., Watts, G.F., Rogers, R.A., and Porcelli, S.A. (2000). Human CD1b and CD1c isoforms survey different intracellular compartments for the presentation of microbial lipid antigens. J. Exp. Med. *192*, 281–288.

20. Sugita, M., Grant, E.P., van Donselaar, E., Hsu, V.W., Rogers, R.A., Peters, P.J., and Brenner, M.B. (1999). Separate pathways for antigen presentation by CD1 molecules. Immunity *11*, 743–752.

21. Moody, D.B., Briken, V., Cheng, T.Y., Roura-Mir, C., Guy, M.R., Geho, D.H., Tykocinski, M.L., Besra, G.S., and Porcelli, S.A. (2002). Lipid length controls antigen entry into endosomal and nonendosomal pathways for CD1b presentation. Nat. Immunol. *3*, 435–442.

22. Cox, D., Fox, L., Tian, R., Bardet, W., Skaley, M., Mojsilovic, D., Gumperz, J., and Hildebrand, W. (2009). Determination of cellular lipids bound to human CD1d molecules. PLoS One *4*, e5325.

23. Haig, N.A., Guan, Z., Li, D., McMichael, A., Raetz, C.R., and Xu, X.N. (2011). Identification of self-lipids presented by CD1c and CD1d proteins. J. Biol. Chem. *286*, 37692–37701. https://doi.org/10.1074/jbc.M111.267948.

24. Yuan, W., Kang, S.J., Evans, J.E., and Cresswell, P. (2009). Natural lipid ligands associated with human CD1d targeted to different subcellular compartments. J. Immunol. *182*, 4784–4791. https://doi.org/10.4049/jimmunol.0803981.

25. Rudolph, M., Wang, Y., Simolka, T., Huc-Claustre, E., Dai, L., Grotenbreg, G., Besra, G.S., Shevchenko, A., Shevchenko, A., and Zeissig, S. (2022). Sortase A-cleavable CD1d identifies sphingomyelins as major class of CD1d-associated lipids. Front. Immunol. *13*, 897873. https://doi.org/10.3389/fimmu.2022.897873.

26. Joyce, S., Woods, A.S., Yewdell, J.W., Bennink, J.R., De Silva, A.D., Boesteanu, A., Balk, S.P., Cotter, R.J., and Brutkiewicz, R.R. (1998). Natural ligand of mouse CD1d1: cellular glycosylphosphatidylinositol. Science *279*, 1541–1544.

27. Rötzschke, O., Falk, K., Deres, K., Schild, H., Norda, M., Metzger, J., Jung, G., and Rammensee, H.G. (1990). Isolation and analysis of naturally processed viral peptides as recognized by cytotoxic T cells. Nature *348*, 252–254.

28. Rudensky, Y., Preston-Hurlburt, P., Hong, S.C., Barlow, A., and Janeway, C.A., Jr. (1991). Sequence analysis of peptides bound to MHC class II molecules. Nature *353*, 622–627.

29. Hunt, D.F., Henderson, R.A., Shabanowitz, J., Sakaguchi, K., Michel, H., Sevilir, N., Cox, A.L., Appella, E., and Engelhard, V.H. (1992). Characterization of peptides bound to the class I MHC molecule HLA-A2.1 by mass spectrometry. Science *255*, 1261–1263.

30. Rammensee, H.G., Falk, K., and Rötzschke, O. (1993). Peptides naturally presented by MHC class I molecules. Annu. Rev. Immunol. *11*, 213–244. https://doi.org/10.1146/annurev.iy.11.040193.001241.

31. Bjorkman, P.J., Saper, M.A., Samraoui, B., Bennett, W.S., Strominger, J.L., and Wiley, D.C. (1987). Structure of the human class I histocompatibility antigen, HLA-A2. Nature *329*, 506–512.

32. Bjorkman, P.J., Saper, M.A., Samraoui, B., Bennett, W.S., Strominger, J.L., and Wiley, D.C. (1987). The foreign antigen binding site and T cell recognition regions of class I histocompatibility antigens. Nature *329*, 512–518. https://doi.org/10.1038/329512a0.

33. Brown, J.H., Jardetzky, T.S., Gorga, J.C., Stern, L.J., Urban, R.G., Strominger, J.L., and Wiley, D.C. (1993). Three-dimensional structure of the human class II histocompatibility antigen HLA-DR1. Nature *364*, 33–39. https://doi.org/10.1038/364033a0.

34. Dendrou, C.A., Petersen, J., Rossjohn, J., and Fugger, L. (2018). HLA variation and disease. Nat. Rev. Immunol. *18*, 325–339. https://doi.org/10.1038/nri.2017.143.

35. Layre, E., Sweet, L., Hong, S., Madigan, C.A., Desjardins, D., Young, D.C., Cheng, T.Y., Annand, J.W., Kim, K., Shamputa, I.C., et al. (2011). A comparative lipidomics platform for chemotaxonomic analysis of *Mycobacterium tuberculosis*. Chem. Biol. *18*, 1537–1549. https://doi.org/10.1016/j.chembiol.2011.10.013.

36. Huang, S., Cheng, T.Y., Young, D.C., Layre, E., Madigan, C.A., Shires, J., Cerundolo, V., Altman, J.D., and Moody, D.B. (2011). Discovery of deoxyceramides and diacylglycerols as CD1b scaffold lipids among diverse groove-blocking lipids of the human CD1 system. Proc. Natl. Acad. Sci. USA *108*, 19335–19340. https://doi.org/10.1073/pnas.1112969108.

37. Willis, R.A., Ramachandiran, V., Shires, J.C., Bai, G., Jeter, K., Bell, D.L., Han, L., Kazarian, T., Ugwu, K.C., Laur, O., et al. (2021). Production of Class II MHC proteins in lentiviral vector-transduced HEK-293T cells for tetramer staining reagents. Curr. Protoc. *1*, e36. https://doi.org/10.1002/cpz1.36.

38. de Jong, A., Peña-Cruz, V., Cheng, T.Y., Clark, R.A., Van Rhijn, I., and Moody, D.B. (2010). CD1a-autoreactive T cells are a normal component of the human alphabeta T cell repertoire. Nat. Immunol. *11*, 1102–1109.

39. Kasmar, A.G., Van Rhijn, I., Magalhaes, K.G., Young, D.C., Cheng, T.Y., Turner, M.T., Schiefner, A., Kalathur, R.C., Wilson, I.A., Bhati, M., et al. (2013). Cutting Edge: CD1a tetramers and dextramers identify human lipopeptide-specific T cells ex vivo. J. Immunol. *191*, 4499–4503. https://doi.org/10.4049/jimmunol.1301660.

40. Ly, D., Kasmar, A.G., Cheng, T.Y., de Jong, A., Huang, S., Roy, S., Bhatt, A., van Summeren, R.P., Altman, J.D., Jacobs, W.R., Jr., et al. (2013). CD1c tetramers detect ex vivo T cell responses to processed phosphomycoketide antigens. J. Exp. Med. *210*, 729–741. https://doi.org/10.1084/jem.20120624.

41. de Jong, A., Cheng, T.Y., Huang, S., Gras, S., Birkinshaw, R.W., Kasmar, A.G., Van Rhijn, I., Peña-Cruz, V., Ruan, D.T., Altman, J.D., et al. (2014). CD1a-autoreactive T cells recognize natural skin oils that function as headless antigens. Nat. Immunol. *15*, 177–185. https://doi.org/10.1038/ni.2790.

42. Wun, K.S., Reijneveld, J.F., Cheng, T.Y., Ladell, K., Uldrich, A.P., Le Nours, J., Miners, K.L., McLaren, J.E., Grant, E.J., Haigh, O.L., et al. (2018). T cell autoreactivity directed toward CD1c itself rather than toward carried self lipids. Nat. Immunol. *19*, 397–406. https://doi.org/10.1038/s41590-018-0065-7.

43. Kasmar, A.G., van Rhijn, I., Cheng, T.Y., Turner, M., Seshadri, C., Schiefner, A., Kalathur, R.C., Annand, J.W., de Jong, A., Shires, J., et al. (2011). CD1b tetramers bind alphabeta T cell receptors to identify a mycobacterial glycolipid-reactive T cell repertoire in humans. J. Exp. Med. *208*, 1741–1747. https://doi.org/10.1084/jem.20110665.

44. Folch, J., Lees, M., and Sloane Stanley, G.H. (1957). A simple method for the isolation and purification of total lipides from animal tissues. J. Biol. Chem. *226*, 497–509.

45. van Meer, G. (2005). Cellular lipidomics. EMBO J. *24*, 3159–3165.

46. Baier, L.J., Sacchettini, J.C., Knowler, W.C., Eads, J., Paolisso, G., Tataranni, P.A., Mochizuki, H., Bennett, P.H., Bogardus, C., and Prochazka, M. (1995). An amino acid substitution in the human intestinal fatty acid binding protein is associated with increased fatty acid binding, increased fat oxidation, and insulin resistance. J. Clin. Invest. *95*, 1281–1287.

47. Cotton, R.N., Wegrecki, M., Cheng, T.Y., Chen, Y.L., Veerapen, N., Le Nours, J., Orgill, D.P., Pomahac, B., Talbot, S.G., Willis, R., et al. (2021).

CD1a selectively captures endogenous cellular lipids that broadly block T cell response. J. Exp. Med. *218*, e20202699. https://doi.org/10.1084/jem.20202699.

48. Sugita, M., Cernadas, M., and Brenner, M.B. (2004). New insights into pathways for CD1-mediated antigen presentation. Curr. Opin. Immunol. *16*, 90–95.

49. Pamer, E., and Cresswell, P. (1998). Mechanisms of MHC class I--restricted antigen processing. Annu. Rev. Immunol. *16*, 323–358.

50. Muindi, K., Cernadas, M., Watts, G.F., Royle, L., Neville, D.C., Dwek, R.A., Besra, G.S., Rudd, P.M., Butters, T.D., and Brenner, M.B. (2010). Activation state and intracellular trafficking contribute to the repertoire of endogenous glycosphingolipids presented by CD1d [corrected]. Proc. Natl. Acad. Sci. USA *107*, 3052–3057. https://doi.org/10.1073/pnas.0915056107.

51. Facciotti, F., Ramanjaneyulu, G.S., Lepore, M., Sansano, S., Cavallari, M., Kistowska, M., Forss-Petter, S., Ni, G., Colone, A., Singhal, A., et al. (2012). Peroxisome-derived lipids are self antigens that stimulate invariant natural killer T cells in the thymus. Nat. Immunol. *13*, 474–480. https://doi.org/10.1038/ni.2245.

52. Birkinshaw, R.W., Pellicci, D.G., Cheng, T.Y., Keller, A.N., Sandoval-Romero, M., Gras, S., de Jong, A., Uldrich, A.P., Moody, D.B., Godfrey, D.I., and Rossjohn, J. (2015). alphabeta T cell antigen receptor recognition of CD1a presenting self lipid ligands. Nat. Immunol. *16*, 258–266. https://doi.org/10.1038/ni.3098.

53. Cotton, R.N., Cheng, T.Y., Wegrecki, M., Le Nours, J., Orgill, D.P., Pomahac, B., Talbot, S.G., Willis, R.A., Altman, J.D., de Jong, A., et al. (2021). Human skin is colonized by T cells that recognize CD1a independently of lipid. J. Clin. Invest. *131*, e140706. https://doi.org/10.1172/JCI140706.

54. Zhou, D., Cantu, C., III, Sagiv, Y., Schrantz, N., Kulkarni, A.B., Qi, X., Mahuran, D.J., Morales, C.R., Grabowski, G.A., Benlagha, K., et al. (2004). Editing of CD1d-bound lipid antigens by endosomal lipid transfer proteins. Science *303*, 523–527.

55. McCarthy, C., Shepherd, D., Fleire, S., Stronge, V.S., Koch, M., Illarionov, P.A., Bossi, G., Salio, M., Denkberg, G., Reddington, F., et al. (2007). The length of lipids bound to human CD1d molecules modulates the affinity of NKT cell TCR and the threshold of NKT cell activation. J. Exp. Med. *204*, 1131–1144. https://doi.org/10.1084/jem.20062342.

56. Kinjo, Y., Wu, D., Kim, G., Xing, G.W., Poles, M.A., Ho, D.D., Tsuji, M., Kawahara, K., Wong, C.H., and Kronenberg, M. (2005). Recognition of bacterial glycosphingolipids by natural killer T cells. Nature *434*, 520–525.

57. Mattner, J., Debord, K.L., Ismail, N., Goff, R.D., Cantu, C., III, Zhou, D., Saint-Mezard, P., Wang, V., Gao, Y., Yin, N., et al. (2005). Exogenous and endogenous glycolipid antigens activate NKT cells during microbial infections. Nature *434*, 525–529.

58. Kain, L., Costanzo, A., Webb, B., Holt, M., Bendelac, A., Savage, P.B., and Teyton, L. (2015). Endogenous ligands of natural killer T cells are alpha-linked glycosylceramides. Mol. Immunol. *68*, 94–97. https://doi.org/10.1016/j.molimm.2015.06.009.

59. Bedard, M., Shrestha, D., Priestman, D.A., Wang, Y., Schneider, F., Matute, J.D., Iyer, S.S., Gileadi, U., Prota, G., Kandasamy, M., et al. (2019). Sterile activation of invariant natural killer T cells by ER-stressed antigen-presenting cells. Proc. Natl. Acad. Sci. USA *116*, 23671–23681. https://doi.org/10.1073/pnas.1910097116.

60. Govindarajan, S., Verheugen, E., Venken, K., Gaublomme, D., Maeleghеer, M., Cloots, E., Gysens, F., De Geest, B.G., Cheng, T.Y., Moody, D.B., et al. (2020). ER stress in antigen-presenting cells promotes NKT cell activation through endogenous neutral lipids. EMBO Rep. *21*, e48927. https://doi.org/10.15252/embr.201948927.

61. Melum, E., Jiang, X., Baker, K.D., Macedo, M.F., Fritsch, J., Dowds, C.M., Wang, J., Pharo, A., Kaser, A., Tan, C., et al. (2019). Control of CD1d-restricted antigen presentation and inflammation by sphingomyelin. Nat. Immunol. *20*, 1644–1655. https://doi.org/10.1038/s41590-019-0504-0.

62. Tian, W., Chen, C., Lei, X., Zhao, J., and Liang, J. (2018). CASTp 3.0: computed atlas of surface topography of proteins. Nucleic Acids Res. *46*, W363–W367. https://doi.org/10.1093/nar/gky473.

63. Mansour, S., Tocheva, A.S., Cave-Ayland, C., Machelett, M.M., Sander, B., Lissin, N.M., Molloy, P.E., Baird, M.S., Stübs, G., Schröder, N.W., et al. (2016). Cholesteryl esters stabilize human CD1c conformations for recognition by self-reactive T cells. Proc. Natl. Acad. Sci. USA *113*, E1266–E1275. https://doi.org/10.1073/pnas.1519246113.

64. Reijneveld, J.F., Marino, L., Cao, T.P., Cheng, T.Y., Dam, D., Shahine, A., Witte, M.D., Filippov, D.V., Suliman, S., van der Marel, G.A., et al. (2021). Rational design of a hydrolysis-resistant mycobacterial phosphoglycolipid antigen presented by CD1c to T cells. J. Biol. Chem. *297*, 101197. https://doi.org/10.1016/j.jbc.2021.101197.

65. Garcia-Alles, L.F., Collmann, A., Versluis, C., Lindner, B., Guiard, J., Maveyraud, L., Huc, E., Im, J.S., Sansano, S., Brando, T., et al. (2011). Structural reorganization of the antigen-binding groove of human CD1b for presentation of mycobacterial sulfoglycolipids. Proc. Natl. Acad. Sci. USA *108*, 17755–17760. https://doi.org/10.1073/pnas.1110118108.

66. Shahine, A., Reinink, P., Reijneveld, J.F., Gras, S., Holzheimer, M., Cheng, T.Y., Minnaard, A.J., Altman, J.D., Lenz, S., Prandi, J., et al. (2019). A T-cell receptor escape channel allows broad T-cell response to CD1b and membrane phospholipids. Nat. Commun. *10*, 56. https://doi.org/10.1038/s41467-018-07898-0.

67. Shahine, A., Van Rhijn, I., Cheng, T.Y., Iwany, S., Gras, S., Moody, D.B., and Rossjohn, J. (2017). A molecular basis of human T cell receptor autoreactivity toward self-phospholipids. Sci. Immunol. *2*, eaao1384. https://doi.org/10.1126/sciimmunol.aao1384.

68. Gras, S., Van Rhijn, I., Shahine, A., Cheng, T.Y., Bhati, M., Tan, L.L., Halim, H., Tuttle, K.D., Gapin, L., Le Nours, J., et al. (2016). T cell receptor recognition of CD1b presenting a mycobacterial glycolipid. Nat. Commun. *7*, 13257. https://doi.org/10.1038/ncomms13257.

69. Tahiri, N., Fodran, P., Jayaraman, D., Buter, J., Witte, M.D., Ocampo, T.A., Moody, D.B., Van Rhijn, I., and Minnaard, A.J. (2020). Total synthesis of a mycolic acid from Mycobacterium tuberculosis. Angew. Chem. Int. Ed. Engl. *59*, 7555–7560. https://doi.org/10.1002/anie.202000523.

70. Cheng, T.Y., Relloso, M., Van Rhijn, I., Young, D.C., Besra, G.S., Briken, V., Zajonc, D.M., Wilson, I.A., Porcelli, S., and Moody, D.B. (2006). Role of lipid trimming and CD1 groove size in cellular antigen presentation. EMBO J. *25*, 2989–2999.

71. Moody, D.B., Reinhold, B.B., Guy, M.R., Beckman, E.M., Frederique, D.E., Furlong, S.T., Ye, S., Reinhold, V.N., Sieling, P.A., Modlin, R.L., et al. (1997). Structural requirements for glycolipid antigen recognition by CD1b-restricted T cells. Science *278*, 283–286.

72. Gilleron, M., Stenger, S., Mazorra, Z., Wittke, F., Mariotti, S., Bohmer, G., Prandi, J., Mori, L., Puzo, G., and De Libero, G. (2004). Diacylated sulfoglycolipids are novel mycobacterial antigens stimulating CD1-restricted T cells during infection with Mycobacterium tuberculosis. J. Exp. Med. *199*, 649–659.

73. Relloso, M., Cheng, T.Y., Im, J.S., Parisini, E., Roura-Mir, C., DeBono, C., Zajonc, D.M., Murga, L.F., Ondrechen, M.J., Wilson, I.A., et al. (2008). PH-dependent interdomain tethers of CD1b regulate its antigen capture. Immunity *28*, 774–786. https://doi.org/10.1016/j.immuni.2008.04.017.

74. Huang, S., Gilfillan, S., Kim, S., Thompson, B., Wang, X., Sant, A.J., Fremont, D.H., Lantz, O., and Hansen, T.H. (2008). MR1 uses an endocytic pathway to activate mucosal-associated invariant T cells. J. Exp. Med. *205*, 1201–1211.

75. Truscott, S.M., Lybarger, L., Martinko, J.M., Mitaksov, V.E., Kranz, D.M., Connolly, J.M., Fremont, D.H., and Hansen, T.H. (2007). Disulfide bond engineering to trap peptides in the MHC class I binding groove. J. Immunol. *178*, 6280–6289. https://doi.org/10.4049/jimmunol.178.10.6280.

76. van't Klooster, J.S., Cheng, T.Y., Sikkema, H.R., Jeucken, A., Moody, B., and Poolman, B. (2020). Periprotein lipidomes of Saccharomyces cerevisiae provide a flexible environment for conformational changes of membrane proteins. eLife *9*, e57003. https://doi.org/10.7554/eLife.57003.

Please cite this article in press as: Huang et al., CD1 lipidomes reveal lipid-binding motifs and size-based antigen-display mechanisms, Cell (2023), https://doi.org/10.1016/j.cell.2023.08.022

CellPress
OPEN ACCESS

STAR★METHODS

KEY RESOURCES TABLE

REAGENT or RESOURCE	SOURCE	IDENTIFIER
Antibodies		
anti-CD1a antibody (clone HI149)	BioLegend	Catalog 300110; RRID AB_314024
purified anti-CD1b (Clone SN13)	BioLegend	Catalog 329102; RRID AB_961143
anti-CD1a (OKT-6, mouse IgG1)	In house aliquots previously tested[36,38]	N/A
anti-CD1b (BCD1b3.1, mouse IgG1)	In house aliquots previously tested[36,38]	N/A
anti-CD1c (F10/21A3, mouse IgG1)	In house aliquots previously tested[36,38]	N/A
anti-CD1d (CD1d42, mouse IgG1)	In house aliquots previously tested[36,38]	N/A
mouse IgG1 isotype control P3	In house aliquots previously tested[36,38]	N/A
Biological samples		
Dulbecco's Modified Eagle Medium	Invitrogen-Gibco	12100-061
RPMI 1640 Medium (Boston)	Gibco	11875-119
fetal bovine serum	Hyclone	SH30071
lipofectamine 2000 Transfection Reagent (Boston)	Invitrogen	11668-027
RPMI 1640 (Melbourne)	Thermo Fisher	21870076
penicillin-streptomycin-glutamine 100x	Gibco	10378016
tobacco etch virus protease	New England Biolabs	P8112S
tobacco etch virus protease reaction buffer (50mM Tris-HCl, 0.5 mM EDTA, 1 mM DTT)	New England Biolabs	B8035S
protein and buffer and crystallization conditions:trizma basesodium chloridepolyethylene glycol 3350sodium iodide	Sigma Sigma Sigma AJAX	T6066 746398 88276 486
3C protease	Pierce	88947
lipofectamine LTX reagent	Invitrogen	15338100
phosphate buffered saline	Lonza AccuGENE	51226
Chemicals, peptides, and recombinant proteins		
diacylglycerol (16:0/18:1)	Avanti polar lipids	800815; 800815C
deoxydihydroceramide (m18:0/16:0)	Avanti polar lipids	860462; 860462P
ceramide (d18:1/18:0)	Avanti polar lipids	860518
lactosylceramide (d18:1/24:0)	Matreya	1507
cardiolipin (18:1)	Avanti polar lipids	790827 discontinued, 710335 as a replacement
phosphatidylethanolamine (16:1/18:1)	Avanti polar lipids	110637 discontinued, 850757 as a replacement
ether-phosphatidylethanolamine (18:0/18:1)	Avanti polar lipids	852758
lyso-phosphatidylethanolamine (18:0)	Avanti polar lipids	856715x
phosphatidylcholine (18:1/16:0)	Avanti polar lipids	850475C
ether-phosphatidylcholine (18:0/18:1)	Avanti polar lipids	852467c
lyso-phosphatidylcholine (24:0)	Avanti polar lipids	855800
deuterated-sphingomyelin (d18:1/16:0D31)	Avanti polar lipids	868584
sphingomyelin (Milk, Bovine)	Avanti polar lipids	860063C
lysosulfatide	Matreya	1904
phosphatidylethanolamine (18:1/16:0)	Avanti polar lipids	850758P
sphingomyelin (d18:1/16:0)	Avanti polar lipids	850584P

(*Continued on next page*)

Please cite this article in press as: Huang et al., CD1 lipidomes reveal lipid-binding motifs and size-based antigen-display mechanisms, Cell (2023), https://doi.org/10.1016/j.cell.2023.08.022

Continued

REAGENT or RESOURCE	SOURCE	IDENTIFIER
isopropanol	Fisher Scientific	A461
methanol	Fisher Scientific	A456
chloroform	Fisher Scientific	C607
water (Optima, LC/MS grade)	Fisher Scientific	W64
hexanes	Fisher Scientific	H303
formic acid	Fisher Scientific	60-006-16
ammonium hydroxide	Fisher Scientific	A470-250
internal calibrants (API-TOF Reference Mass Solution)	Agilent	G1969-85001
recombinant HLA-B2705 (HIV gag peptide KRWIILGLNK-loaded monomer)	NIH tetramer core	HLA-B2705 (peptide-loaded monomer)
recombinant CD1a	NIH tetramer core	hCD1a
recombinant CD1b	NIH tetramer core	hCD1b
recombinant CD1c	NIH tetramer core	hCD1c
recombinant CD1d	NIH tetramer core	hCD1d
recombinant Mamu A01 (rCMV20 peptide VTPPELIL-loaded monomer)	NIH tetramer core	Mamu A01 (peptide-loaded monomer)
polybrene	Sigma-Aldrich	H9268
puromycin	Sigma-Aldrich	P8833
imidazole ≥99% (titration), crystalline	Sigma-Aldrich	I0250-25G
Critical commercial assays		
Ni-NTA superflow nickel-charged resin	Qiagen	30410
Strep-Tactin sepharose superflow	IBA Life Science	2-1208-010
pLV lentiviral vector (four-plasmid lentiviral system)	Biosettia	cDNA-pLV07
baculovirus expression: *Trichoplusia ni* High Five cellsInsect-XPRESS medium	Gibco Lonza	B85502 12-730F
SDS-PAGE reagents:40% Acrylamide/ Bis solution (37.5: 1), 40% (w/v) Sodium dodecyl sulfate, Lauryl	Astral ScientificSigma	BIOA00008-500ML 151-21-3
HiLoad Superdex S200 1660 (size exclusion chromatography)	Cytiva	28989335
HiTrap Q HP 1mL (anion exchange chromatography)	Cytiva	17115301
Phastgel isoelectric focusing gel (IEF) 4-6.5	Cytiva	17054401
MagStrep type3 XT beads (Oxford)	IBA Lifesciences	2-4090-002
Deposited data		
CD1b-lysosulfatide (8GLE)	PDB protein bank (www.rcsb.org/)	PDB: 8GLE
CD1b-SM (8GLF)	PDB protein bank (www.rcsb.org/)	PDB: 8GLF
CD1b-PE (8GLG)	PDB protein bank (www.rcsb.org/)	PDB: 8GLG
CD1b-endoPC (8GLH)	PDB protein bank (www.rcsb.org/)	PDB: 8GLH
CD1b-GMM (8GLI)	PDB protein bank (www.rcsb.org/)	PDB: 8GLI
Experimental models: Cell lines		
K562 cells	In house aliquots previously tested[36,38]	N/A
293T cells	In house aliquots previously tested[36,38]	N/A
THP-1 cells	ATCC	tib-202
Experimental models: Organisms/strains		
XL2-Blue ultracompetent cells (E. coli)	Agilent (Stratagene)	200150

(*Continued on next page*)

Please cite this article in press as: Huang et al., CD1 lipidomes reveal lipid-binding motifs and size-based antigen-display mechanisms, Cell (2023), https://doi.org/10.1016/j.cell.2023.08.022

Continued

REAGENT or RESOURCE	SOURCE	IDENTIFIER
Recombinant DNA		
pMXIP (pMX.IRES.Puromycin)	In house aliquots previously tested[74]	N/A
pLV lentiviral vector	Biosettia	cDNA-pLV07
Gag-pol	Invitrogen	pLP1
Rev	Invitrogen	pLP2
VSV-G	Invitrogen	pLP/VSVG
Software and algorithms		
MassHunter software	Agilent	https://www.agilent.com/en/product/software-informatics/mass-spectrometry-software
XCMS (version 1.24) for R platform	Scripps research institute	http://bioconductor.org/packages/release/bioc/html/xcms.html
Venny program	BioinfoGP Service	https://bioinfogp.cnb.csic.es/tools/venny/
Limma (linear models for microarray data) for R platform	Bioconductor	https://bioconductor.org/packages/release/bioc/html/limma.html
iMosflm	MRC Laboratory of Molecular Biology	https://www.mrc-lmb.cam.ac.uk/harry/imosflm/ver730/introduction.html
Aimless (CCP4i program suite)	Collaborative Computational Project No. 4 Software for Macromolecular X-Ray Crystallography	https://www.ccp4.ac.uk/
coot graphics program	MRC Laboratory of Molecular Biology	https://www2.mrc-lmb.cam.ac.uk/personal/pemsley/coot/
phenix-refine	Phenix project - Lawrence Berkeley Laboratory	https://phenix-online.org/
PyMOL 2.1.1.	Schrödinger, Inc.	https://pymol.org/2/
CONTACT (CCP4i program suite)	Collaborative Computational Project No. 4 Software for Macromolecular X-Ray Crystallography	https://www.ccp4.ac.uk/
CASTp 3.0 server	Wei Tian, Chang Chen, and Jieling Zhao	http://sts.bioe.uic.edu/castp/
Other		
MONOCHROM DIOL column (3 μm X 150 mm X 2 mm)	Fisher Scientific- Varian	50-010-4901 and A0542150X020 discontinued; InfinityLab Poroshell 120 as replacement
MetaGuard guard column	Varian	A0542-MG2
Poroshell EC-C18 column	Fisher Scientific-Agilent Technologies InfinityLab	NC1483109
Blue Sepharose® 6 Fast Flow	Cytiva	17-0948-01

RESOURCE AVAILABILITY

Lead contact

Requests for resources are directed to D. Branch Moody: bmoody@bwh.harvard.edu.

Materials availability

- Plasmids and cell lines for expressing CD1 proteins will be available upon request.
- Purified human CD1 proteins are available from the NIH Tetramer Facility.

Data and code availability

- CD1b crystal structures with endogenous ligands have been deposited to the Protein DataBank (PDB): 8GLE, 8GLF, 8GLG, 8GLH, 8GLI.
- All original code for differential abundance analysis and PCA is available as an R Markdown present in Dataset S1.

- Lipidomics datasets are provided in full for all ligands in Tables S1 and S2.
- All data reported in this paper will be shared by the lead contact upon request.

Additional data

- Any additional information required to reanalyze the data reported in this paper is available from the lead contact upon request.

EXPERIMENTAL MODEL AND STUDY PARTICIPANT DETAILS

Human cell culture

We expressed CD1 proteins in hematopoietic (K562), human embryonic kidney (293T), and human myeloid phagocytic (THP-1) cell lines. K562 and THP-1 cells were generally grown in DMEM culture medium, whereas 293T was grown in RPMI 160 culture medium, supplemented with 5% fetal bovine serum. K562 and THP-1 Cells were routinely maintained in flasks and were expanded to large volumes in roller bottles to express a large amount of CD1 protein.

METHOD DETAILS

CD1 and MHC expression

We expressed 'linked' and 'unlinked' CD1 and MHC proteins in Boston and Atlanta, respectively. Linked CD1-β2m complexes were connected via the N-terminus of each heavy chain with the C-terminus of β2m using a flexible peptide linker. HLA-B2705 contained an additional linker to tether the HIV gag peptide KRWIILGLNK.[75] Transmembrane and cytoplasmic domains of heavy chains were replaced with strep-tag II and octahistidine tags for the affinity purification from hematopoietic cell line K562.[38] Unlinked CD1-β2m complexes were generated for T cell recognition as described.[37,39,40,43] The transmembrane and cytoplasmic regions were removed and the heavy chain was modified with an αZipper, BSP85, and hexahistidine tag. The C-termini of β2m was extended with a linker and a β Zipper sequence, and a cleavable *Thosea asigna virus* 2A peptide, allowing the separation of the heavy chain from β2m. Upon expression, CD1a, CD1b and CD1c heavy chains and β2m can reassemble through the interaction of αZipper and βZipper sequences at their C-termini. Mamu A01, an MHC class I protein from rhesus macaque was refolded using an *E.coli* expression system with an rCMV20 peptide VTPPELIL. For CD1d, constructs did not use zippered domains.

The antigen presenting function of linked proteins in K562 cells was equivalent to native CD1 proteins in dendritic cells[38]. Linked protein purification from the culture supernatant of K562 cells was analyzed as detailed previously[36] using an ELISA with monoclonal antibodies OKT-6 (anti-CD1a), BCD1b3.1 (anti-CD1b), F10/21A3 (anti-CD1c), CD1d42 (anti-CD1d), and P3 (mouse IgG1 control). Proteins were purified with affinity chromatography using Ni-NTA agarose resin (Qiagen) and Strep-Tactin sepharose (IBA Lifescience). Unlinked CD1 proteins collected from the culture supernatant of 293T cells using the hexahistidine tag and Ni-NTA agarose.[43] The yield and purity of purified proteins were confirmed with an SDS-PAGE gel and Coomassie blue staining. Proteins were extracted in chloroform: methanol: water (2:2:1) (V: V: V) (Figure S1) at room temperature for 30 mins and centrifuged at 500g for 10 mins. The aqueous phase contained few lipids, so the combined interphase and organic phase were transferred and stored at -20°C for comparative lipidomics analysis, which was conducted in parallel with groups of lipid extracts.

For cleavable CD1b, 293T cells were co-transfected with the four-plasmid lentiviral system (Biosettia) containing the cleavable CD1b-β2m gene with a TEV protease site, and vectors containing Gag-pol, Rev and VSV-G (Invitrogen), along with transfection reagent Lipofectamine 3000 (ThermoFisher). Cells were grown in RPMI 1640 (Thermo Fisher) supplemented with 10% fetal bovine serum (FBS) and penicillin-streptomycin-glutamine (ThermoFisher) for 5 days, when the supernatant was filtered (0.45 μM) and transferred to 293T cells in fresh culture media. Polybrene (50 μg, Sigma-Aldrich) was added to the supernatant, which was added to 2 x 10^6 K562 or THP-1 cells and grown in a T25 flask overnight. K562 or THP-1 supernatant was removed, discarded and replaced with the 293T supernatant and cultured for 4 days. Cells were washed in fresh culture media and with PBS, followed by analysis on a BD LSR II or LSRFortessa X20 and sorted by purified anti-CD1b (Clone SN13; Biolegend) on a BD FACSAria III with FACSDiva software (BD Immunocytometry Systems). $CD1b^+$ cells were expanded in high glucose DMEM + 5% FBS for three days in roller bottles. Cells were harvested and washed in PBS, before resuspending in 10mL TEV protease reaction buffer and incubating 24 hours at 4C with 100 U of TEV protease. Cell debris were pelleted by centrifugation and supernatant was filtered (0.45 μM) and diluted to 100 mL in 50 mM Tris-HCl pH 8.0, 500 mM NaCl, 20 mM imidazole, before purification by a nickel affinity chromatography and Strep-Tactin XL Sepharose resin as done with the soluble CD1b construct. Sample purity was analysed by SDS-PAGE, and purified proteins were buffer exchanged into PBS and concentrated for mass spectrometry analysis.

For cleavable CD1a, the extracellular domain and transmembrane domain were separated by a TEV cleaving site, Strep-tag II, and HRV 3C cleavage site. The β2m was linked to CD1a sequences with a furin glycine-serine linker and porcine teschovirus 2A self-cleaving peptides. The K562 cell line was transduced and stability selected in puromycin (20 mg/ml, Gibco). K562 cells (~$2x10^8$) were harvested and subjected to HRV 3C protease (Pierce) digestion at 4C overnight. The cleaved CD1a was purified from the filtered digestion supernatants (50 mL) by immobilization onto 100 μl MagStrep XT beads (IBA Lifesciences) at 4C overnight with gentle rotation. For truncated CD1a, CD1a transmembrane domain was removed and replaced with an AviTag, HRV 3C cleavage site, 8xHis-Tag and twin Strep-tag II. K562 cell line was transfected using Lipofectamine LTX Reagent (Invitrogen). Five days later,

supernatant containing truncated CD1a was collected, filtered and serum albumin were removed by Blue Sepharose column (Cytiva) before concentration to 50 mL using Vivaspin Centrifugal Concentrator (10kDa, Sartorius). Truncated CD1a was purified from the concentrated supernatants (50 mL) by immobilization onto 100 μl MagStrep XT beads (IBA Lifesciences) at 4C overnight with gentle rotation. For quantitation, biotinylated CD1a protein was immobilized onto 20 μl beads in 10 mL PBS (Lonza AccuGENE) at 4C overnight with gentle rotation. Bead-bound CD1a was washed three times with PBS and the protein concentrations were determined with FACS staining using APC anti-CD1a antibody (HI149, BioLegend) with an external standard curve and stored at -20°C.

Mass spectrometry-based comparative lipidomics

Lipid eluents were annormalized to protein mass (20-80 μg), dried under nitrogen at 20°C, dissolved and briefly sonicated in starting mobile phase, which was 100% solvent B containing 70% hexanes, 30% isopropanol, 0.1% formic acid, and 0.05% ammonium hydroxide. Triplicate samples for each protein analyzed with blanks that were intermixed and monitored for lipid carryover, using an Agilent 1200 series HPLC autosampler with an Agilent 6520 Accurate-Mass Q-TOF MS controlled by MassHunter software. A normal phase gradient with solvent A (70% isopropanol, 30% methanol, 0.1% formic acid, and 0.05% ammonium hydroxide) and solvent B through a MonoChrom Diol column (3 μm X 150 mm X 2 mm; Varian, A0542150X020) were connected to a MetaGuard guard column (2 mm, Varian, A0542-MG2). The binary gradient was monitored with solvent B with 100% at 0-10 min, 50% at 17-22 min, 0% at 30-35 min, and 100% at 40-50 min, followed by an additional 6 min post-run for regeneration. Ionization occurred with a dual-electrospray ionization source maintained at 325°C with a drying gas flow of 5 L/min, nebulizer pressure of 30 pounds per square inch, and a capillary voltage of 5.5 kV. Positive- and negative-ion modes were typically monitored between *m/z* 100-3000 with the acquisition rate of 1.4 spectra/sec and 713.7 ms/spectrum. Internal calibrants (Agilent G1969-85001, *m/z* 121.050573, 922.009798) were continuously monitored to assess electrospray efficiency and mass accuracy. NanoESI-CID-MS was typically performed at a collision energy of 35V and an isolation width of 1.3 *m/z* and adjusted to optimize signal during individual experiments. For the semi-quantitative analysis of PCs and SMs eluted from cleavable CD1, the lipid eluents were normalized based on input protein and 10 μl were injected into a reverse-phase HPLC-MS system (Agilent Poroshell EC-C18 column, 1.9-micron, 3 x 50 mm with an Agilent 6520 QTOF mass spectrometry).[76]

Lipidomic analyses

Mass profiles were initially visualized and manually compared using MassHunter software and then converted into an mzData format as input files for further quantitative analyses of detected peaks. XCMS (version 1.24) using the R platform with the centWave algorithm for peak finding and the intensity-weighted mean algorithm was used for peak quantification. Lipidomes were aligned across using a signal-to-noise threshold of 10, *m/z* deviation of 10 parts per million, a frame width of mzdiff of 0.001, a peak width of 10–120 s, and a bandwidth of 5. To detect ion finding errors such as split peaks, chromatograms were extracted using MassHunter to manually inspect the curve shapes. Venn diagrams were made in Venny.

Chemical annotation of molecular features

One lead compound in each lipid class was studied with authentic standards from Avanti Lipids, where available, including diacylglycerol (M=594.522, #800815), deoxydihydroceramide (M=523.533, #860462), ceramide (M=565.543, #860518), lactosylceramide (M=959.727, Matreya# 1507), cardiolipin (M=1457.034 #790827), PE (M=717.531, #110637), EPE (M=729.567, #852758), LPE (M=481.317, #856715x), deuterated-PC (M=790.772, #860399), EPC (M=771.614, # 852467c), lyso-PC (M=607.458, #855800) and deuterated-SM (M=733.762, #868584).

Determination of media lipid binding

We measured exchange of exogenous lipids by adding H^2-labeled PC (16:0D31/18:1) and SM (d18:1/16:0D31) (Avanti) at concentrations equivalent to those from 5 % FBS (Hyclone). The cell culture with H^2-labeled lipids was processed in parallel to regular cultures for cell harvest, protein purification, and lipidomic analyses.

Structural characterization of CD1b presenting SM, lysosulfatide, PE, endogenous PC, and GMM C85

The CD1b-β2m complex was purified as previously described.[67] Briefly, CD1b from the baculovirus expression system was made in *Trichoplusia ni* High Five cells. Secreted CD1b is purified to homogeneity via nickel-chelating metal affinity chromatography and size exclusion chromatography. For hybrid complex formation, CD1b is first treated with a molar excess of C18:1 lysosulfatide (Matreya) in 0.5%, and purified by anion exchange chromatography, then subsequently loaded with C34 PE and C34 SM (Avanti), or synthetic GMM C85 prepared in 0.5 % tyloxapol and 5 % CHAPS hydrate, and validated by isoelectric focusing gel (IEF). These 'hybrid' complexes carrying exogenously loaded self-lipids, as well as CD1b-endogenous (unloaded) binary structures were generated via the vapor diffusion hanging drop method, with drops formed at a 1:1 ratio between protein at 5mg.mL^{-1} in 10 mM Tris-HCl pH 8.0 and 150 mM NaCl, and the mother liquor comprising 22% PEG 3350 and 0.1 M NaI. Crystals of diffraction quality were flash frozen in liquid nitrogen and data collection was conducted at the Australian Synchrotron MX1 beamline. Data was processed using iMosflm and Aimless in the CCP4i program suite. Crystal structures were solved by molecular replacement, using CD1b-phosphatidylglycerol as the model (PDB: 5WL1). Manual adjustment of these models was conducted in the coot graphics program, followed by maximum-likelihood refinement with phenix-refine. Molecular representations were generated in PyMOL 2.1.1. Contacts were analysed using

the CONTACT program in the CCP4i program suite. The final crystal structures were deposited in the Protein Data Bank, with the following accession codes: CD1b-lysosulfatide (8GLE), CD1b-SM (8GLF), CD1b-PE (8GLG), CD1b-endogenous PC (8GLH), and CD1b-GMM (8GLI).

Consensus cleft volume calculations

Antigen binding cleft volumes were calculated via the CASTp 3.0 server with a probe radius of 1.7Å, using Cononley's solvent-excluded surface volume equation.[62]

QUANTIFICATION AND STATISTICAL ANALYSIS

Statistical analyses were performed using MassHunter (Agilent) and XCMS to generate p-values from triplicate runs using ANOVA analysis. Principal components analysis of linked and unlinked proteins used the subset of differentially abundant lipids with Benjamini Hochberg-adjusted $p < 0.05$ based on the F-statistic after all pairwise contrasts. A bubble plot of lipids with differential abundance found in all lipidomes showed their relative abundance in each CD1 isoform.

CellPress
OPEN ACCESS

Supplemental figures

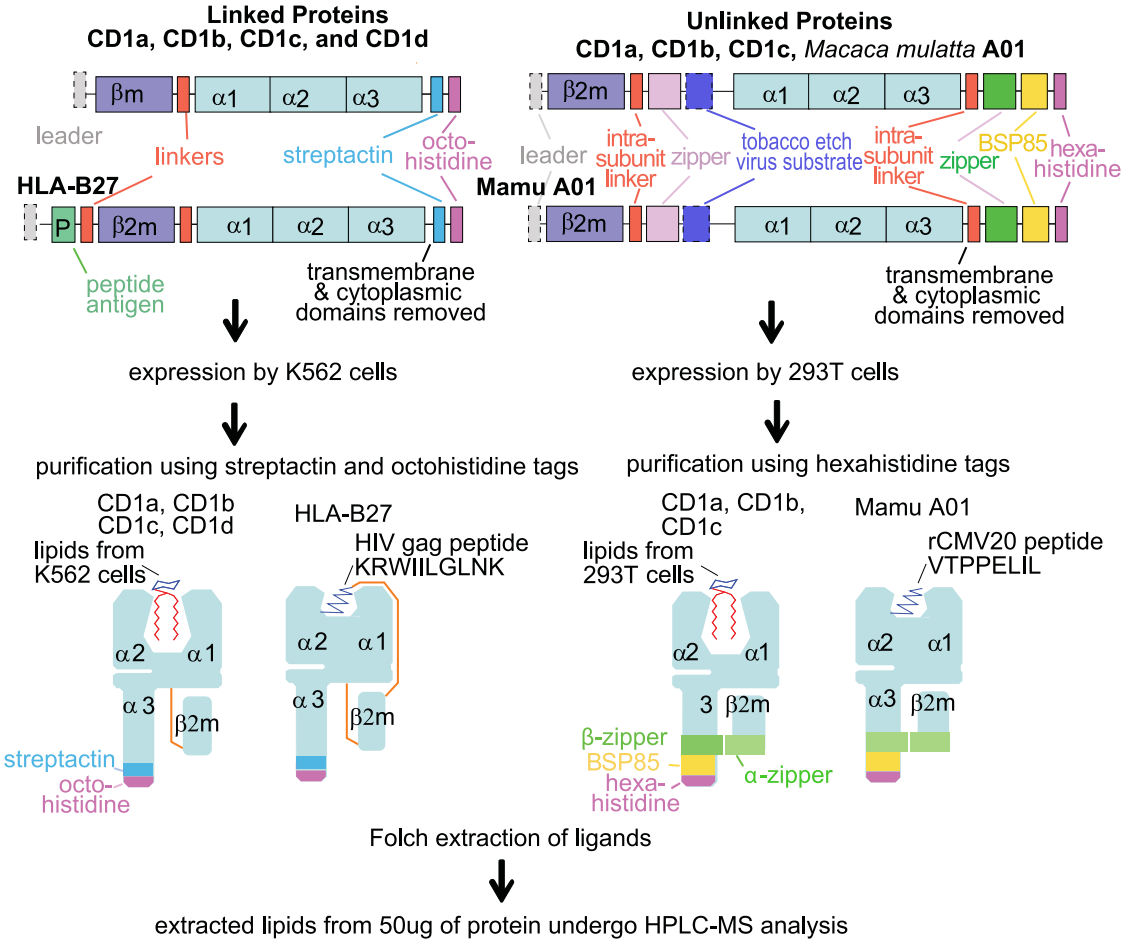

Figure S1. Schematic of CD1 expression, related to Figures 1, 2, and 3

Unlinked CD1d was constructed without a zipper region, and T2A is a peptide (P) from *Thosea asigna* virus. BSP85 is a substrate peptide 85 for *E. coli* biotin ligase BirA. rCMV20 is a recombinant cytomegalovirus peptide.

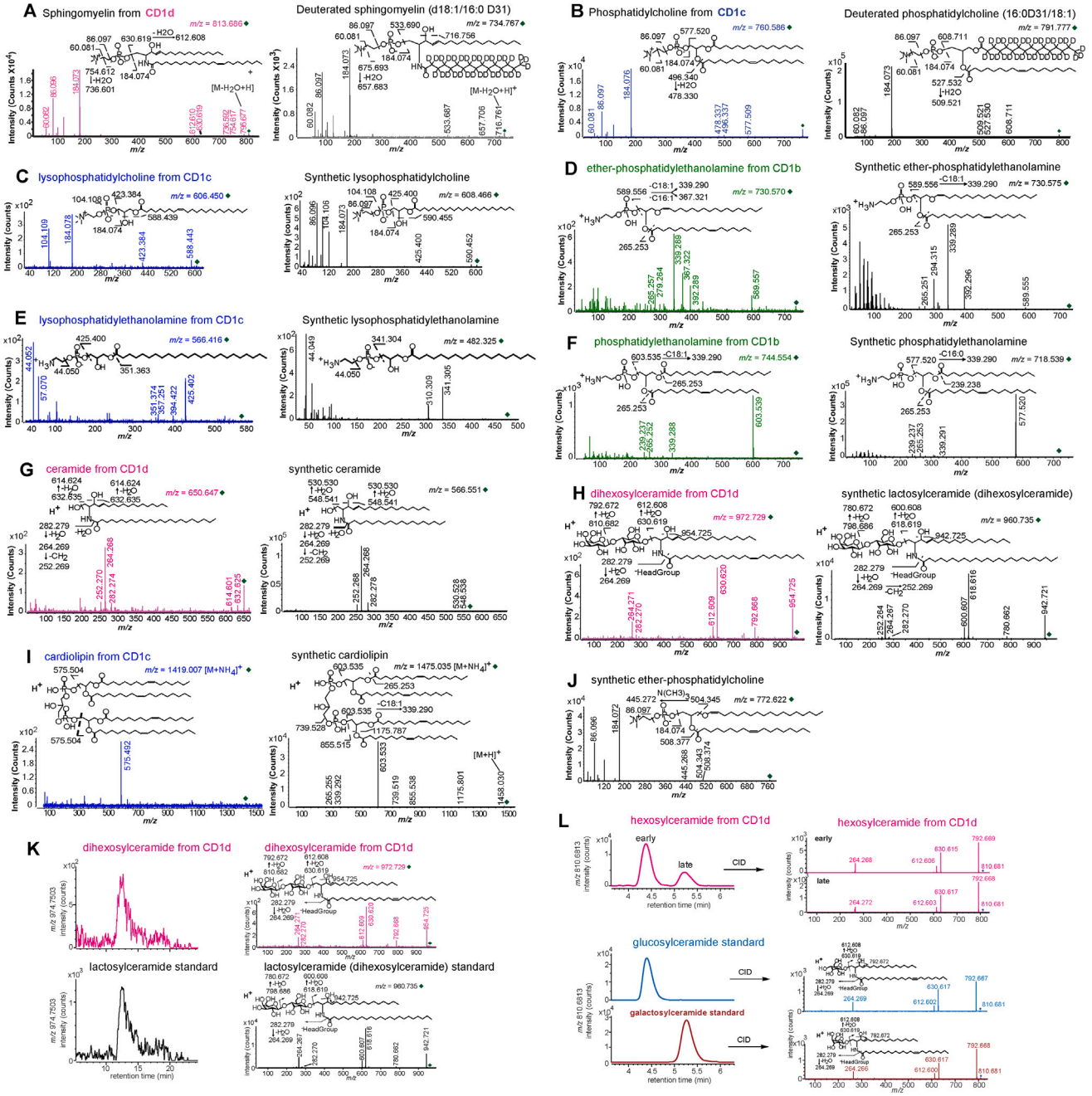

Figure S2. CID-MS of CD1-associated lipids, related to Figures 1, 4, and 5

(A and B) Eluted endogenous and deuterium-labeled exogenous lipids were distinguished based on mass, and their structures were confirmed in CID-MS.

(C–J) Synthetic standards and native lipids eluted from CD1 proteins were collided to generate diagnostic ions.

(K) Dihexosylceramide from CD1d coeluted with lactosylceramide and showed equivalent CID-MS spectra.

(L) Hexosylceramides from CD1d showed two peaks, which coeluted with β-glucosylceramide and β-galactosylceramide, respectively.

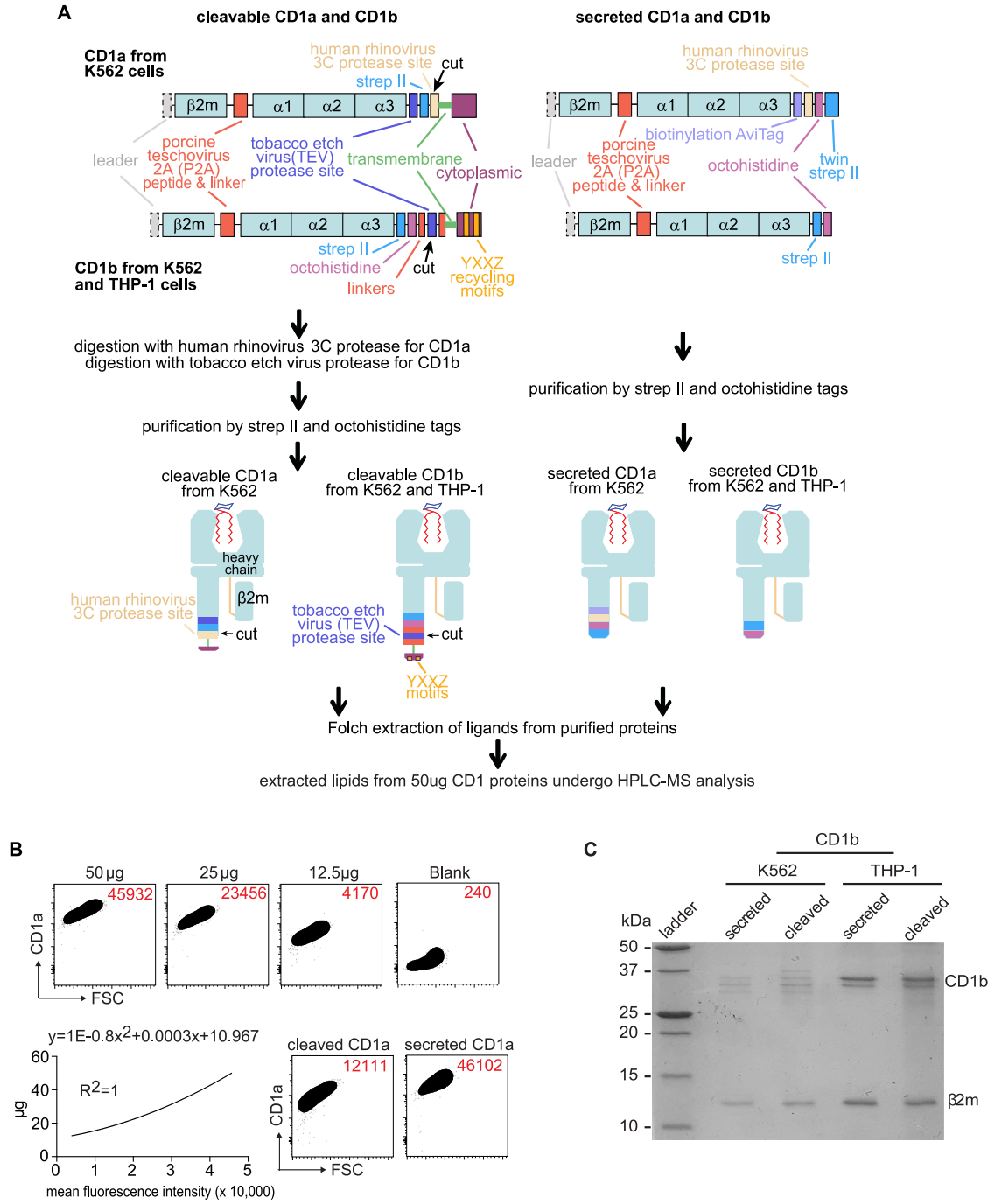

Figure S3. Recombinant CD1a andCD1b proteins, related to Figure 3

(A) Schematic of CD1b protein design, cleavage, capture and elution. (B) Flow cytometry of capture beads carrying cleaved or secreted human CD1a proteins was quantitated with an external CD1a standard. (C) CD1b proteins in polyacrylamide gel electrophoresis show β2-microglobulin and the glycosylated CD1b heavy chain.

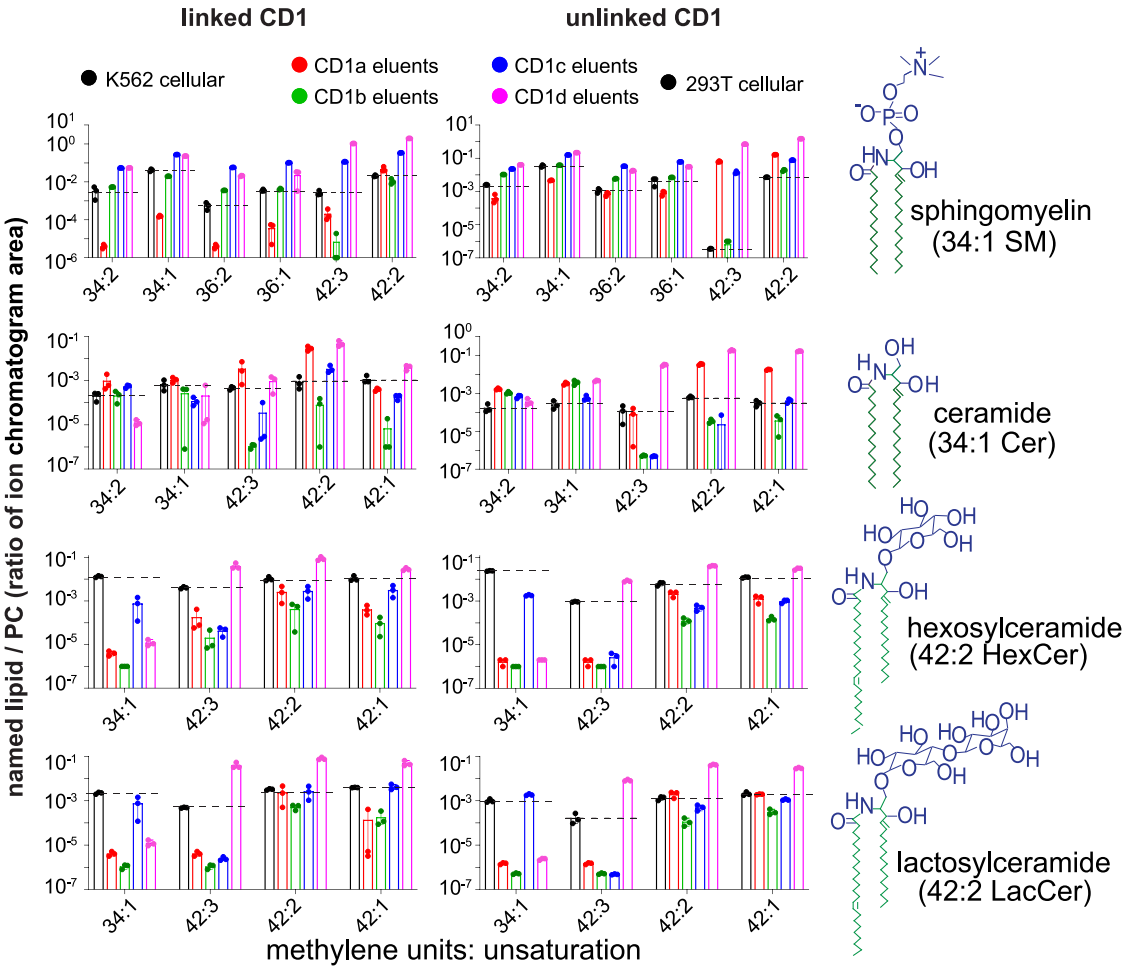

Figure S4. Chain length analysis of sphingolipids bound to CD1, related to Figure 5

Each lipid is designated according to the combined chain length and unsaturation of its sphingosine and alkyl chains.

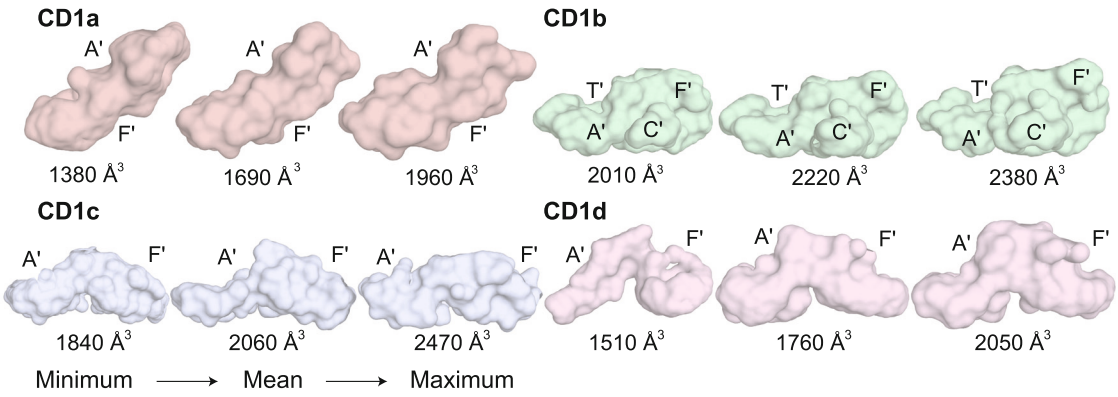

Figure S5. Variability in CD1 cleft volume, related to Figure 6

Representative cleft surface traces depict volumes (in Å^3) for previously solved CD1 structures.

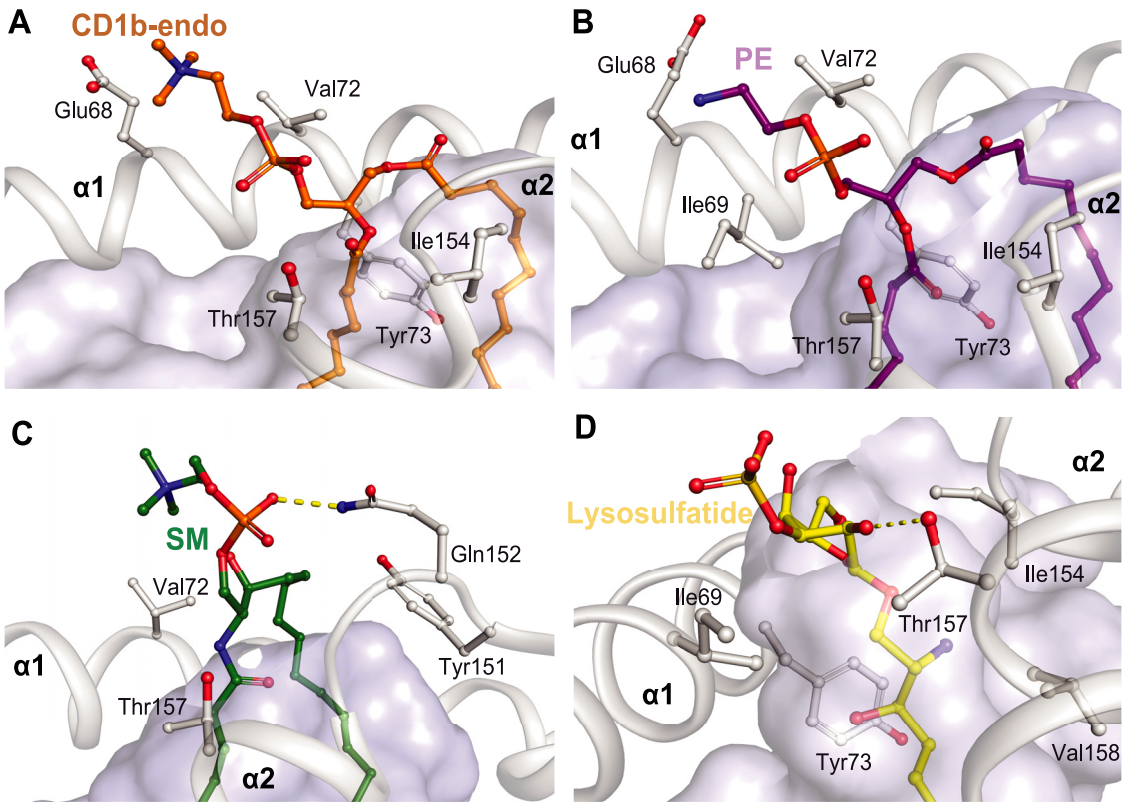

Figure S6. CD1b contacts with self antigen headgroups, related to Figure 7

Contacts between CD1b (gray) and endogenous (endo) lipids (A), PE (B), SM (C), and lysosulfatide (D) are highlighted. Hydrogen bonds are yellow dashes, with sulfur, nitrogen, and oxygen colored in orange, blue, and red respectively.

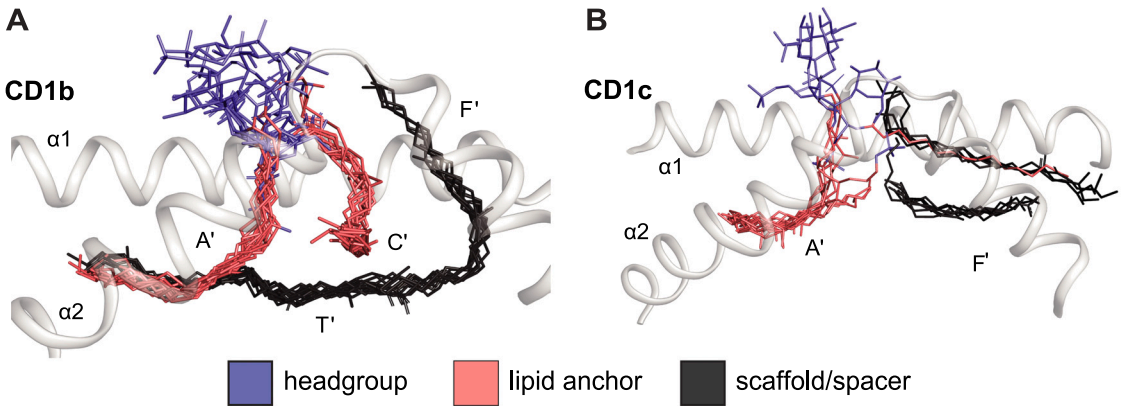

Figure S7. Lipid placement in CD1b and CD1c, related to Figure 7

(A) In conventional views with antigen headgroups shown at the top of images, overlay of 13 CD1b published crystal structures demonstrates "consensus" binding sites for the head group and lipid anchor of the antigenic lipid, which are positioned above scaffold lipids.

(B) Overlay of 5 CD1c structures demonstrates less conserved placement of lipids, with mostly side-to-side positioning.